nature materials

SUPPLEMENTARY INFORMATION

DOI: 10.1038/NMAT4570

Biodegradable scaffold with built-in vasculature for organ-on-a-chip engineering and direct surgical anastomosis

Boyang Zhang[1,2], Miles Montgomery[1,2], M. Dean Chamberlain[2], Shinichiro Ogawa[3], Anastasia Korolj[1], Aric Pahnke[1,2], Laura A. Wells[2], Stéphane Massé[4], Jihye Kim[5], Lewis Reis[2], Abdul Momen[6], Sara S. Nunes[6], Aaron Wheeler[1,5], Kumaraswamy Nanthakumar[4], Gordon Keller[3], Michael V. Sefton[1,2] and Milica Radisic[1,2,7]*

[1]Department of Chemical Engineering, University of Toronto, Toronto, Ontario, Canada. [2]Institute of Biomaterials and Biomedical Engineering, University of Toronto, Toronto, Ontario, Canada. [3]McEwen Center for Regenerative Medicine, Toronto, Ontario, Canada. [4]The Toby Hull Cardiac Fibrillation Management Laboratory, Toronto General Hospital, Toronto, Ontario, Canada. [5]Department of Chemistry, University of Toronto, Toronto, Ontario, Canada. [6]Toronto General Research Institute, University Health Network, Toronto, Ontario, Canada. [7]The Heart and Stroke/Richard Lewar Centre of Excellence, Toronto, Ontario, Canada. *e-mail: m.radisic@utoronto.ca

Table of Contents

Supplementary Methods

Nuclear magnetic resonance (NMR) spectroscopy and Fourier transform infrared spectroscopy (FT IR) of POMaC bulk polymer: 1D 1H CPMGT2 spectrum was acquired at 25ºC on an Agilent DD2 spectrometer operating at 699.806MHz for 1H (Agilent, Walnut Creek, CA). The spectrometer was equipped with a 5mm HFCN Cold Probe. The spectrum was acquired over a 11160.7Hz spectral window with 100446 points, a 10s recycle delay, 2 steady state scans, and 16 transients using a 200ms CPMGT2 filter. NMR processing was carried out using MNova software (v. 9.0.0, Santiago de Compostela, Spain). Briefly, the spectrum was Fourier transformed, phased, and baseline corrected prior to analysis. Transmission spectra were obtained using an ATR top-plate accessory coupled to a Spectrum One FTIR spectrometer with a fast recovery deuterated triglycine sulfate detector (PerkinElmer, Inc., Waltham, MA). The spectra were recorded in the region between 4000 and 650cm^{-1}.

Mechanical properties of POMaC bulk polymer. A four-factor design of experiment (DOE) of 2^4=16 samples was conducted to demonstrate the range of mechanical properties that POMaC can achieve. The effects of UV energy, heat, citric acid to maleic anhydride monomer ratio (CA:MA), and porogen content on the mechanical properties of POMaC were studied. The physical range of the factors is shown in **Table 1**. A center point with four replicates was added to the experiment to improve model accuracy, for a total of twenty samples.

The twenty samples were prepared in random order from three batches of pre-polymer (the liquid POMaC pre-polymer before curing), where each batch corresponds to a level for monomer feed ratio: 0.25, 0.875, and 1.5 CA:MA. Each batch had 5% of photoinitiator compound added to it. Batches were divided with different proportions of porogen added. The high and low levels were split to contain either 0% or 60% porogen, and the middle level batch had 30% porogen added. UV energy was delivered in proportion to the weight percentage of POMaC, as outlined in **Table 2**. Pre-cured samples were injected into PDMS moulds (n>3 replicates per measurement) with dimensions of 10mm×1.5mm×0.1mm and cured as appropriate. Tensile tests were conducted on all samples to obtain the range of the material's Young's Moduli.

Supplementary Table 1: Summary of low, high, and midpoint levels for the DOE

Level	UV Exposure (**Factor A**)	Duration of Heat Exposure (**Factor B**)	Monomer ratio (CA:MA) (**Factor C**)	% Porogen (**Factor D**)
Low (-)	1600-4000 mJ	1 day	0.25	0%
Middle (m)	7700 mJ	2 days	0.875	30%
High (+)	7200-18000 mJ	3 days	1.5	60%

Supplementary Table 1: UV exposure for different levels of porosity

Porogen %	**UV exposure (mJ)**		
	low	middle	high
high: 60%	1600	-	7200
middle: 30%	2800	7700	12600
low: 0%	4000	-	18000

AngioChip fabrication tips: When curing PDMS against the silicon mould, it is crucial to cure the PDMS at room temperature (**Supplementary Figure 3 (step 2)).** This is because the later alignment step, which aligns two PDMS moulds together, was performed at room temperature. Due to the thermo expansion effect, if the PDMS mould was cured at a high temperature, its overall size would be reduced once cooled down to a room temperature. The degree of reduction could vary between different moulds and result in size mismatch during alignment **(Supplementary Figure 3 (step 5))**. This mismatch would become very pronounced when multiple scaffolds were aligned at the same time across a large mould surface area. PDMS should also be prepared with 1:15 cross-linker ratio. Stiffer PDMS moulds could prevent the scaffold from releasing and transferring to the glass slides **(Supplementary Figure 3 (step 5)).**

When injecting POMaC solution through the PDMS mould, it is critical to apply gentle pressure to prevent the mould from delaminating from its substrate. For a mould with simple features, a drop of POMaC solution can be applied at the inlet to allow capillary action to take up the solution and fill the mould overnight. For more complex designs manual injection via a syringe pump might be necessary (**Supplementary Figure 3 (step 4)).** Incorporation of porogen (PEGDM) in POMaC makes the polymer solution less viscous hence greatly improving the injection efficiency. Solvents such as DMSO and dioxane that react with PDMS should not be used.

In this work, a high amount of UV photoinitiator at 5% (w/w) was used in the POMaC solution. Therefore, controlling and fine-tuning the UV exposure energy is critical to partially cure the polymer. Excessive UV exposure in **step 4** of **Supplementary Figure 3** could result in failure of bonding in **step 5** of **Supplementary Figure 3**. For the multi-layer scaffold, which requires multiple bonding steps, reducing UV photoinitiator would help avoid over-UV-exposure. Over-UV-exposure would result in stiff and brittle scaffolds with prolonged degradation time. For multi-layer scaffold, after **step 5** of **Supplementary Figure 3**, the patterned POMaC base layer on the glass slide can be further baked for 5min on 120℃ hot plate to improve the adhesion between the POMaC base layer and the glass slide. This step prevents the base layer lifting from the glass slide prematurely in the subsequent steps, hence making the process more robust. This is especially helpful for thick scaffold fabrication due to the multiple bonding steps. Once each scaffold layer is properly bonded, the bonding is strong enough to withstand sterilization in 70% ethanol solution, which would swell the scaffold significantly but without delaminating the scaffold.

Scanning electron microscopy of AngioChip scaffold. To illustrate the structure of the AngioChip, AngioChip scaffolds were imaged with Hitachi SEM S-3400 prior to porogen leaching. Cutting the scaffold transversely revealed the cross section. To image the nano-pores of the scaffolds, after porogen leaching in PBS, the scaffolds were first dehydrated in ethanol and then prepared with supercritical point drying hence preventing the collapsing of the nano-pores structure and gold coating prior to imaging.

Micro computed tomography (MicroCT) of AngioChip scaffold. To visualize the internal architecture of the AngioChip scaffolds, µCT40 (Scanco medical) was used to scan the scaffolds that were anchored onto a polystyrene slide. The program µCT Ray V40 was used to apply a threshold to the acquired images to eliminate background and reconstruct the scaffold in 3-D. To visualize the internal built-in network of the scaffold, the network was filled with barium sulphate suspension (105%(w/v), Polibar plus, Therapex) mixed with 2%(w/v) gelatin in PBS (porcine skin, type A, Sigma) at 1:1(v/v) ratio. The injected solution was allowed to gel at room

temperature and imaged with μCT, where a threshold was applied to the acquired image to reveal the built-in network against the other structure of the scaffold.

AngioChip scaffold degradation. To prepare the nano-porous scaffold samples, scaffolds (3mm×10mm×200μm) with 60% porogen content were UV cross-linked for 4 min at intensity of 10mJ/cm^{2}s and weighted. To prepare the pore-free scaffold samples, scaffolds (3mm×10mm×200μm) with 0% porogen content were UV cross-linked for 10 min at intensity of 10mJ/cm^{2}s and weighted. The degradation rates of the scaffolds were determined by tracking the scaffold mass loss over time in PBS (pH 7.4, 37°C) or in 0.1 M NaOH. After each incubation period, the samples were first thoroughly washed with distilled water and then dried. The mass loss was calculated by comparing the initial mass with the mass measured at the specific time point.

AngioChip burst pressure. To determine the burst pressure of the AngioChip scaffolds without micro-holes, the inlet of the scaffold was connected to a nitrogen tank with a pressure gauge using Tygon tubing, while the outlet of the scaffold was sealed with epoxy glue. Pressure was increased gradually until a leak was observed from the scaffold network and the peak pressure was recorded as the burst pressure. If a leak from the junctions at the inlet or the outlet was observed first, the recording was discarded.

AngioChip scaffold and myocardium mechanical testing. The mechanical properties of the AngioChip scaffold were measured in PBS with a Myograph (Kent Scientific) in the circumferential (along the long edge) and longitudinal direction (along the short edge) of the AngioChip scaffolds. Strain-to-failure values were determined from the strain at the breaking point along the curves. The effective elasticity of the adult rat myocardium was measured from the adult hearts of Lewis rats, sacrificed according to a protocol approved by the University of Toronto Animal Care Committee. The adult rat myocardium was sliced into 7mm long strips with a width of 2-4mm and thickness of 2-4mm along the circumferential direction or longitudinal direction of the heart.

The rat myocardium was only stretched up to 20% strain because the stress-strain curve of the myocardium becomes nonlinear outside of the 20% strain region as shown in other studies[1]. In addition, normal heart physiological strain from active contraction is only within 15%[2]. The AngioChip scaffolds were stretched until break, a strain much higher than 20%, in order to determine the ultimate tensile strength. The effective elasticity of both the scaffold and the myocardium was derived from the slope of the stress-strain curve between 0% to 10%, consistent with previous studies[1] (**Supplementary Figure 9, 10**).

Anisotropic ratio was determined by dividing the effective elasticity in the circumferential direction with the effective elasticity in the longitudinal direction. The three different scaffold designs (**Figure 2a-c**) had different lattice structures but the same built-in network with a wall thickness of 50μm, an inner luminal dimension of 50μm by 200μm for the inlet, outlet and first order branch, and an inner luminal dimension of 50μm by 100μm for the second order branch. The scaffold lattice was made of 50μm struts. In design A, the struts were spaced 250μm apart in the long-edge direction, 100μm apart in the short-edge direction, and they were continuous in the z-axis. In design B, the struts were spaced 250μm apart in the long-edge direction, 100μm apart in the short-edge direction, and 50μm apart in the z-axis. In design C, the struts were spaced 550μm apart in the long-edge direction, 175μm apart in the short-edge direction, and 50μm apart in the z-axis.

AngioChip permeability. The permeability of large molecules (TRITC-Dextran, ~70 kDa, Sigma) from the built-in network of the micro-hole free AngioChip, AngioChip with 10µm micro-holes, or AngioChip that was both endothelialized and contained 10µm micro-holes was measured. TRITC-Dextran was perfused at 0.7µL/min through the network with inlet concentration of 10 µM for 20hr. After 20 hr, the solution in the middle wells was collected and the concentration of fluorescent molecules was correlated to a standard curve determined with a fluorescence plate-reader. The channel permeability of the entire AngioChip scaffold to large molecules was determined from the net rate of diffusion (total accumulated fluorescent molecules in the middle chamber/time) and the luminal surface area of the network, using Fick's Law with the assumption that the average concentration of fluorescent molecules inside the network is the same to that at the inlet. To illustrate diffusion and metabolism of biomolecules in the tissue space, 100µM carboxyfluorescein diacetate (CFDA, 557 Da) in PBS was perfused at 0.7µL/min through the scaffold network with 10µm micro-holes surrounded by cardiac cells (1 day after seeding) for 60min.

POMaC material biocompatibility *in vivo*: Poly-L-lactic acid (PLLA, 85,000-160,000Da, Sigma) was first dissolved in cholorform. POMaC pre-polymer was prepared as described above. PLLA solution and POMaC solution were then cast into a disk-shaped mould with diameter of 8mm and height of 1mm. PLLA disks were formed by evaporating the solvent overnight. POMaC disks were formed by UV-exposure at an intensity of 10mJ/cm^{2}s for 4min. Both PLLA disks and POMaC disks were sterilized in 70% ethanol and repeatedly washed in ethanol and deionized water prior to implantation. PLLA and POMaC disks were subcutaneously implanted for 5 weeks in adult male Lewis rats. Explanted tissues were formalin fixed, paraffin embedded, sectioned and stained for H&E, Masson's Trichrome, CD3, CD68, and CD163 at the Pathology Research Program (PRP) at the University Health Network. Tissue sections were scanned and cells within 200µm (400pixels) from the implant surface were quantified for positive staining of Masson's Trichrome, CD3, CD68, or CD163.

Quantification of cell density in AngioChip tissues. Cell density was quantified from histology sections based on previously described stereology method[3] according to the following formula:

$$N_V = N_A/(t+D) \qquad \text{(Eq. 1)}$$

where N_V is the number of nuclei per unit volume, N_A is number of nuclei per unit area on a histology section, t is the section thickness corrected for tissue shrinkage, and D is the average diameter of cell nuclei. First, the average cell nuclei diameter was determined from confocal images. The average diameter of at least 40 nuclei was used. The number of nuclei per unit area on the randomly selected areas of the cross-section of the AngioChip tissues was determined from 3µm thick histology sections. The micro-channel area was excluded from the area calculation. A correction factor of 5.7% reported previously[3] was used to account for tissue shrinkage during tissue preparation for histology. For hepatic tissues, density was quantified for the AngioChips containing hESC-hepatocytes and 20% of human MSCs in the parenchyma. For cardiac tissues, density was quantified for the AngioChips based on hESC-derived CMs.

Histology and immunofluorescent staining. Immuno-fluorescent staining was performed to assess the morphology of cultivated AngioChip tissues. The AngioChip cardiac tissues and the Biowire or monolayer

controls were first fixed in 4% (w/v) paraformaldehyde in PBS for 15min at room temperature. Then, the tissues were permeated *in situ* and blocked with 5% FBS and 0.25% Triton×100 in PBS for 1 hour. Next, the AngioChip cardiac tissues were incubated in primary antibody, sarcomeric α-actinin (Mouse, 1:200 dilution, Sigma) overnight at 4˚C, followed by incubation with corresponding secondary antibodies, Alexa 488 anti-mouse IgG (1:200 dilution, Sigma) or TRITC anti-mouse (1:200 dilution, Sigma) and F-actin (Phalloidin 660 conjugated, Sigma) for 1hour. The cardiac tissues were imaged with Olympus FV5-PSU confocal microscope with 10× and 40× objectives. The AngioChip hepatic tissues and the collagen sandwich controls were first fixed in 4% (w/v) paraformaldehyde in PBS for 15min at room temperature. Then the tissues were permeated in cold methanol on ice for 2min. Next, the tissues were incubated in primary antibody, E-cadherin (Mouse, 1:200 dilution, BD Biosciences) and Albumin (Goat, 1:200 dilution, Bethyl) overnight at 4˚C, followed by incubation with corresponding secondary antibodies, Alexa 647 anti-mouse IgG (1:200 dilution, Sigma) and TRITC anti-goat (1:200 dilution). Prior to fixation, some hepatic tissues were incubated with Carboxy-DCFDA (5µM, Life Technologies) in HBSS (with Ca^{2+}/Mg^{2+}) for 20min as described to visualize bile canaliculi[6]. Carboxy-DCFDA is a substrate of MRP2, a hepatocyte efflux transporter, thus it can be used to observe the canalicular uptake and efflux, as well as to label the bile canaliculi structures, crucial in the transport of bile acid from hepatocytes to bile ducts[6]. To visualize the vasculature, endothelialized AngioChip scaffolds were stained with CD31 (Mouse, 1:200 dilution, Sigma), followed by Alexa 647 anti-mouse IgG (1:200 dilution, Sigma) as described previously[4]. Live and dead staining was performed with carboxyfluorescein diacetate (CFDA, 1:1000 dilution, Invitrogen) and propidium iodide (PI, Invitrogen) in PBS at 37˚C for 30min. To visualize the cross-section of the cardiac tissue with live and dead staining, the tissues were sliced in half transversely and rotated manually to show the cross-section. To visualize both endothelial cells and parenchymal cells, cultivated tissues were fixed in 10% formalin for 3 days at 4˚C, paraffin embedded, and sectioned into 3µm slices for histology at the Pathology Research Program Laboratory of Toronto University Health Network. Histology sections show the tissue cross-section in the transverse direction and were stained with Hematoxylin and Eosin (H&E), Masson's Trichrome stain, CD31, or albumin.

Urea assay on hepatic tissue: The AngioChip hepatic tissues were incubated with 1mL hepatocyte media, containing 10mM ammonium bicarbonate, in the main wells and perfused with 1mL endothelial cell media, containing 10mM ammonium bicarbonate, from the inlet wells. After 24hr incubation, the media from the main wells and the outlet wells were collected. The media were briefly centrifuged (300×g for 5min) to remove any cells and frozen at -20˚C. Urea was detected using QuantiChrom Urea assay kit (BioAssay Systems) as per the manufacturer's instructions. The media were typically used undiluted for detection. The media baseline reading for urea was determined from media collected at the same perfusion condition but without the presence of liver cells in the AngioChip scaffold. To quantify cell number of AngioChip tissue and collagen sandwich culture, the tissues were first ground and the cells were lysed in cell lysis buffer (Cell Signaling). The supernatant was collected and analyzed with Quant-iT™ PicoGreen® dsDNA Assay Kit according to manufacturer's instruction and correlated to a standard curve.

Liver drug test. On day 3 of culture**,** terfenadine (10µM, Sigma) in hepatocyte culture media was placed in the inlet wells and perfused through the endothelialized hepatic tissue at 0.7µL/min (0.62dynes/cm^2, Re, 0.01) for 24hr. After 24hr incubation, the media in the inlet wells, middle wells, and outlet wells were

collected and analyzed for the concentration of fexofenadine with Liquid Chromatography–Mass Spectrometry (LC-MS) and correlated to a standard curve. DMSO was used to dissolve the drugs initially. The final concentration of DMSO in the media was always less than 0.1%.

Lactate dehydrogenase (LDH) assay on cardiac tissue: The AngioChip cardiac tissues were cultured with cardiomyocyte media with or without media perfusion through the built-in network at 0.7μL/min (0.62dynes/cm^2, Re, 0.01). From the middle wells where the tissues resided, 1mL of cardiomyocyte media was collected and replaced with new media every day for 6 days. The collected media were analyzed for lactate dehydrogenase (LDH) concentration with a LDH toxicity assay kit (Cayman Chemical) as per manufacturer's instructions and correlated to a standard curve.

Cardiac drug test. On day 7 of culture, the spontaneous contractions of the cardiac tissues were recorded as brightfield videos. Then, epinephrine (10μM, Sigma) or digoxin (10μM, Sigma) in cardiac culture media were placed in the inlet wells and perfused at 0.7μL/min (0.62dynes/cm^2, Re, 0.01) through the endothelialized cardiac tissue for 30min. After 30min incubation, the spontaneous contractions of the cardiac tissues were recorded again as brightfield videos. The frequency of contraction was analyzed from the recorded videos with Image J. DMSO was used to dissolve the drugs. The final concentration of DMSO in the culture media was diluted to less than 0.1% (v/v).

Functional characterization of engineered cardiac tissue. To stimulate the AngioChip cardiac tissue and measure their electrical excitability parameters, two carbon electrodes spaced 1cm apart were placed within each main well on the opposite sides of the tissue in parallel. The electrodes were connected to an external electric stimulator (Grass s88x) with platinum wires. Using monophasic pulses of 2ms duration and frequency of 1 pulse per second, the excitation threshold (minimum voltage at which synchronous contractions of 75% of the tissue in the field of view can be observed) was first determined. Then the maximum capture rate (maximum beating frequency) was determined at 200% of the determined excitation threshold voltage. The amplitude of the tissue contraction was determined from the change of width in the engineered tissue between contractions normalized to the tissue width at the relaxed state. To track the process of tissue remodeling, a bright-field image of the AngioChip cardiac tissue was taken daily in the first 5 days after cell seeding (Olympus SC30 camera). For the purpose of comparison with other published studies and to quantify the gel compaction rate for the rat and human cardiac constructs, the AngioChip tissue area was measured from brightfield images at different time points. Conduction velocity was assessed upon staining the tissues with a voltage sensitive dye, Di-4-ANNEPS, as we described previously[5].

Supplementary Results

POMaC degradation properties, mechanical properties, and rationale for selection

Degradation in PBS is commonly employed to measure the degradation rates of hydrolytically degradable polymers, such as POMaC[7], *in vitro*. Accelerated degradation at high pH is usually performed to confirm that the bonds that participate in hydrolysis are accessible within the biomaterial. The AngioChip scaffolds degraded gradually in phosphate buffered saline (PBS) over months and to completion in 3 days under alkaline conditions (0.1M NaOH) (**Supplemental Figure 8a,b**), time-frames that were consistent with those reported previously for the base material used in AngioChip production, POMaC[7].

By varying the UV energy (factor A), heat exposure time (factor B), monomer ratio (factor C) and porogen concentration (factor D), we were able to vary the POMaC bulk polymer elasticity over a wide range (**Supplementary Table 3**) and come up with an empirical equation, using a design of experiment (DOE) approach, that enables us to fine-tune the mechanical properties for future applications.

Supplementary Table3: Summary of the average Young moduli values at different experimental conditions

-,+, m refer to the low, high and middle levels of the four experimental parameters as shown for DOE in the **Supplementary Table 1**.

Young's Modulus					
Sample	UV	Temperature	CA:MA ratio	% Porogen	Modulus (kPa)
1	-	-	-	-	0
2	+	-	-	-	411 ± 109
3	-	+	-	-	53 ± 8
4	-	-	+	-	329 ± 119
5	-	-	-	+	256 ± 74
6	+	+	-	-	1240 ± 577
7	+	-	+	-	406 ± 100
8	+	-	-	+	996 ± 296
9	-	+	+	-	951 ± 211
10	-	+	-	+	464 ± 177
11	-	-	+	+	152 ± 34
12	+	+	+	-	1423 ± 651
13	+	+	-	+	736 ± 108
14	+	-	+	+	630± 125
15	-	+	+	+	248 ± 27
16	+	+	+	+	436 ± 23
17	m	m	m	m	1036 ± 276
18	m	m	m	m	942 ± 187
19	m	m	m	m	1359 ± 475
20	m	m	m	m	970 ± 74
Random Testing Order: 7, 12, 15, 18, 3, 13, 10, 11, 9, 17, 20, 2, 5, 8, 6, 4, 19, 1, 16, 14					

DOE approach enabled us to detect the main effects of the four factors investigated as well as the presence of

interactions between the factors. A least squares analysis of the Young's Modulus (YM) produced the following equation:

$$YM = b_o + b_A x_A + b_B x_B + b_C x_C + b_D x_D + b_{AB} x_A x_B + b_{AC} x_A x_C + b_{AD} x_A x_D + b_{BC} x_B x_C + b_{BD} x_B x_D + b_{CD} x_C x_D + b_{ABC} x_A x_B x_C + b_{ABD} x_A x_B x_D + b_{ACD} x_A x_C x_D + b_{BCD} x_B x_C x_D + b_{ABCD} x_A x_B x_C x_D + \varepsilon \quad \textbf{(Eq.2)}$$

where b_n are the coefficients determined from fitting the linear least squares model to Eq. 2. x_n are the dependent variables of the model in coded units (i.e. -1 to 1) consistent with the values shown in the **Supplementary Table 1**, with the subscript n referring to A=UV energy, B=heat duration, C=CA:MA monomer ratio and D=porogen content.

A simplified partial model reduced the equation to:

$$YM_{partial} = b_o + b_A x_A + b_B x_B + b_{BD} x_B x_D + b_{CD} x_C x_D + b_{ABD} x_A x_B x_D + \varepsilon \quad \textbf{(Eq.3)}$$

where only the significant effects (i.e. $p < 0.05$) were included. In Eq. 3, b_n coefficient subscripts are labelled as follows: o=intercept of the model, A=UV energy, B=heat duration, BD=interaction between heat duration and porogen content, CD=interaction between monomer ratio and porogen content, ABD=interaction between UV energy, heat direction, and porogen content and ε is the residual.

The coefficients for the partial model are shown in **Supplementary Table 4**.

Supplementary Table 4: Coefficients for the DOE model

Coefficients				
	Estimate	**Std. Error**	**t-value**	**Pr(>|t|)**
b_o	690.25	49.85	13.845	$< 2\times10^{-16}$
b_A	211.4	57.82	3.656	0.000647
b_B	136.67	57.99	2.357	0.022656
b_{BD}	-154.97	58.03	-2.671	0.010365
b_{CD}	-137.44	58.03	-2.368	0.022027
b_{ABD}	-140.32	57.95	-2.422	0.019366

The results demonstrated that the Young's modulus directly depended on the UV exposure and the thermal crosslinking times, while porogen content exhibited interactive effects with both heat exposure time and monomer ratio. The model also detected an interactive effect of three independent factors: UV crosslinking time, heat exposure and porogen content.

Trends for the main factor effects were as expected. Over the ranges investigated, UV energy had the

greatest positive influence on the Young's Modulus. The UV photoinitiator induces free radical polymerization by attacking the vinyl groups of the maleic anhydride. Temperature increases the Young's Modulus as ester bonds between free carboxylic acids and hydroxyl groups increase the degree of crosslinking.

POMaC was therefore selected due to elasticities, ranging from 53-1423kPa, favorable for soft tissue applications (**Supplementary Figure 8c, Supplementary Table 3**) and documented blood compatibility of citric acid-based elastomers[8,9]. FDA approved polyesters poly(lactic acid), poly(glycolic acid), poly(ε-caprolactone) and their co-polymers are significantly more stiff (Young's moduli range from 0.1GPa to 10 GPa[10]) and brittle, thus they are not suitable for AngioChip production for the purpose of soft tissue engineering. Additionally, they are not suitable for manufacturing of blood contacting devices and vascular tissue engineering as they are thrombogenic[11] without additional modification. Here, we demonstrated AngioChip production from POMaC, but we propose that other scaffold materials might be used in the future as long as they satisfy the general criteria of tissue specific elasticity and non-thrombogenicity.

Culture medium distribution in AngioChip scaffold compartments

To characterize culture medium flow in different compartments, 4mL of PBS was loaded into the inlet well and 1mL in the main well of the multi-well plate, where an AngioChip scaffold with 10μm holes was placed. The PBS was allowed to perfuse through the AngioChip for a total of 24hr, at which point the PBS was collected from the inlet, main and the outlet wells for the purpose of closing the mass balance on the perfused fluid. As illustrated in the **Supplementary Figure 8d**, most of the perfused fluid ended up in the outlet well as expected. Specifically at 24hr, there was 2.7±0.2mL in the inlet well, 1.2±0.1mL in the main well and 1.1±0.1mL in the outlet well, indicating there was no significant leakage of the fluid into the tissue space, even without the presence of endothelial cells in the AngioChip lumen.

Diffusivity in AngioChip parenchymal space

We observed transient FITC diffusion from the outer AngioChip channel lumen through the parenchymal layer and into the media reservoir, which behaved as an infinite sink since the volume of the media was 67 times greater than the AngioChip volume. Fluorescence intensity profiles were obtained using Image J at the mid-line of the AngioChip, perpendicular to the channel wall, 20min and 30min after initiation of FITC perfusion (10μM in PBS). Focusing on the diffusion from the outer channels, it was possible to apply the theory for transient diffusion in the semi-infinite media, as described[12]. Using this approach the diffusion coefficient for FITC in the parenchymal space was estimated to be $3.4\text{-}3.8\times10^{-11} m^2/s$, only slightly lower than the diffusion coefficient of FITC in PBS as reported previously ($2.7\times10^{-10} m^2/s$)[13], indicating that the polymer lattice in the parenchymal layer did not dramatically hinder solute diffusion.

Rationale for selection of micro-hole sizes

The micro-hole sizes of 10μm and 20μm were selected to enable cell extravasation from the main AngioChip vasculature into the parenchymal space. The micro-holes of 10μm in diameter and 50μm in spacing were selected to enable monocyte extravasation based on their size and a previously published microfluidic lung-on-a-chip[14] that included a membrane with 10μm micro-holes spaced 40-50μm apart, which allowed robust transmigration of monocytes (12μm in diameter for THP-1 monocytes[15]) in previous studies[14] as well as

here (**Figure 3 m-r**). Micro-holes of 20μm in diameter were selected to allow robust endothelial sprouting since small capillaries can range from 5-10μm in diameter. We found that within micro-holes of 20μm in diameter, multiple endothelial cells could wrap into a tubular structure (**Figure 3e-g**).

Polymer biocompatibility

At 5 weeks post sub-cutaneous implantation in a rat model, both poly-L-lactic acid (PLLA) and POMaC scaffolds were visible at the implantation site, indicating POMaC did not biodegrade fully over 5 weeks. Qualitatively, the appearance of histology sections of PLLA and POMaC from the biocompatibility study was similar (**Supplementary Figure 26**). POMaC exhibited less fibrosis in comparison to PLLA, as assessed by collagen coverage from Mason's Trichrome staining (**Supplementary Figure 26**). Quantification of immunostaining for macrophage and T-cell specific markers demonstrated that although there were more M2, pro-healing, macrophages with the POMaC scaffold implantation, there were also more T-cells in this group compared to the PLLA group. The ratio of pro-healing to total macrophages was similar in the PLLA and POMaC groups. Further studies are necessary to delineate similarities between PLLA and POMaC responses at different times post implantation, to evaluate the contribution of different scaffold elasticities to the observed responses, as well as to determine the time required for the complete degradation of both scaffolds in this animal model.

Cell culture considerations for construction of mm-thick tissues

We made two simple modifications to our culture procedure developed for the single-layer AngioChip tissues in order to improve both cell density and organization in thick multi-layer AngioChip tissues: 1) We used centrifugation assisted cell seeding to seed cells uniformly in the entire volume of a 3-layer AngioChip scaffold and 2) We extended the liquid reservoir in the AngioChip bioreactor to achieve a higher pressure head and a higher perfusion rate (11.7 ± 3.6 mL/day, n=4). For seeding of thin tissues, we used a simple pipetting for cell seeding and lower pressure heads (i.e. perfusion rates, 1.1 ± 0.1mL/day) that were not sufficient to support cell growth in the thick multi-layer scaffolds. We also waited for a minimum of 3 days in perfusion culture to assess cell distribution and organization in these high-density constructs (**Figure 5q-w**, **Supplementary Figure 19, 20**). Our previous work conclusively showed that in the thick high-density tissues with insufficient oxygen and nutrient supply (i.e. tissues cultured under static conditions), massive cell death occurred within a period of hours (e.g. 4.5 hr[16]) after seeding of metabolically active cells such as cardiomyocytes, resulting in the inability of the cells in the scaffold interior to elongate and a non-uniform cell distribution (i.e. a void interior)[16,17]. Centrifugation assisted seeding is critical for uniform initial cell distribution in thick scaffolds and providing sufficient pressure head is critical for proper tissue perfusion. In principle, these factors can be tuned for tissues of thickness greater than 2mm as described here using scalable AngioChip-based techniques that rely on multi-layer scaffolds with one inlet and one outlet, or on the stacking of individual single-layer AngioChip tissues to make a thicker structure.

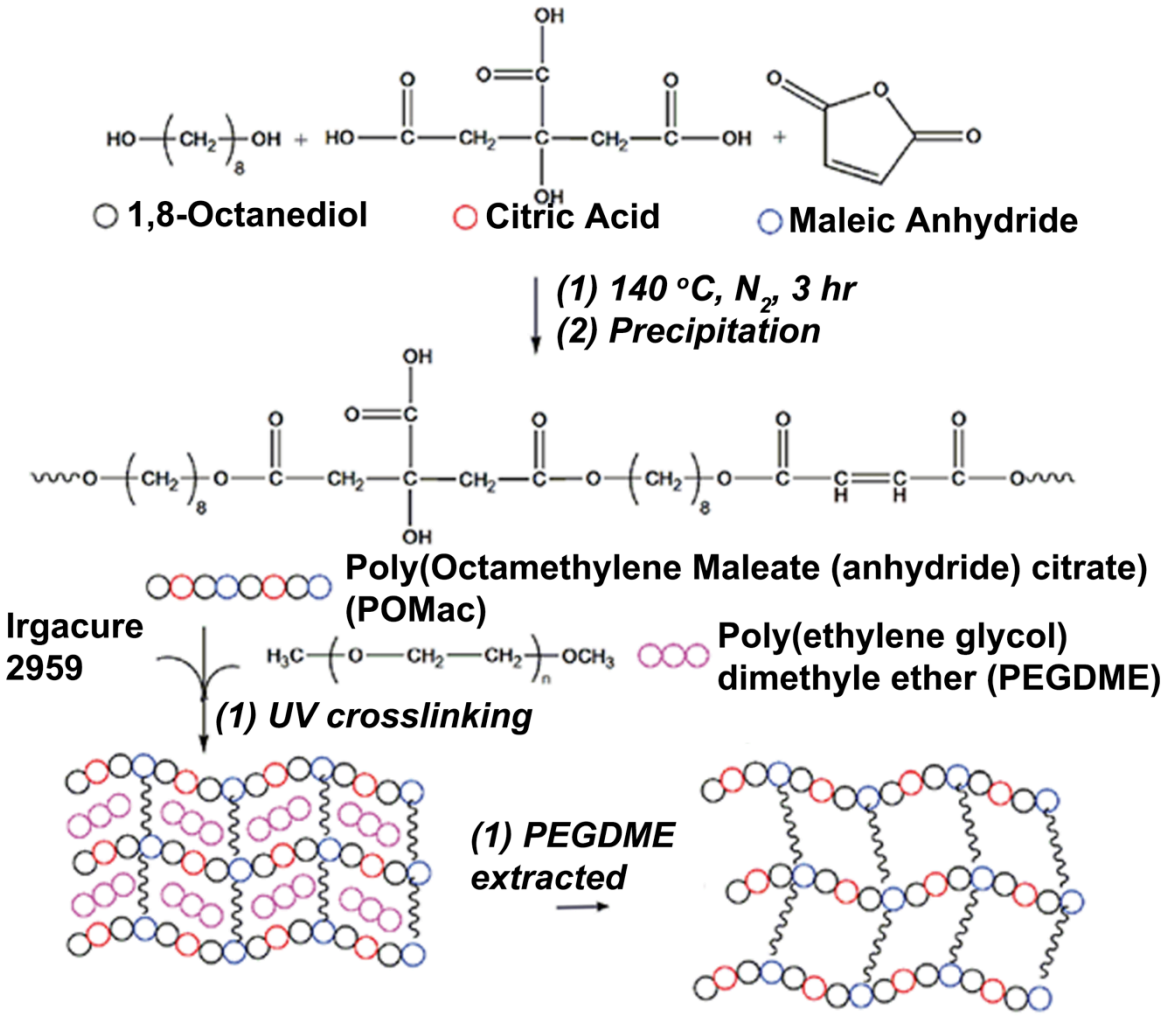

Supplementary Figure 1. Schematics of chemical synthesis of the POMaC pre-polymer.
Synthesis of cross-linked POMaC polymer involving poly-condensation, photo-crosslinking mechanism, and PEGDME porogen leaching.

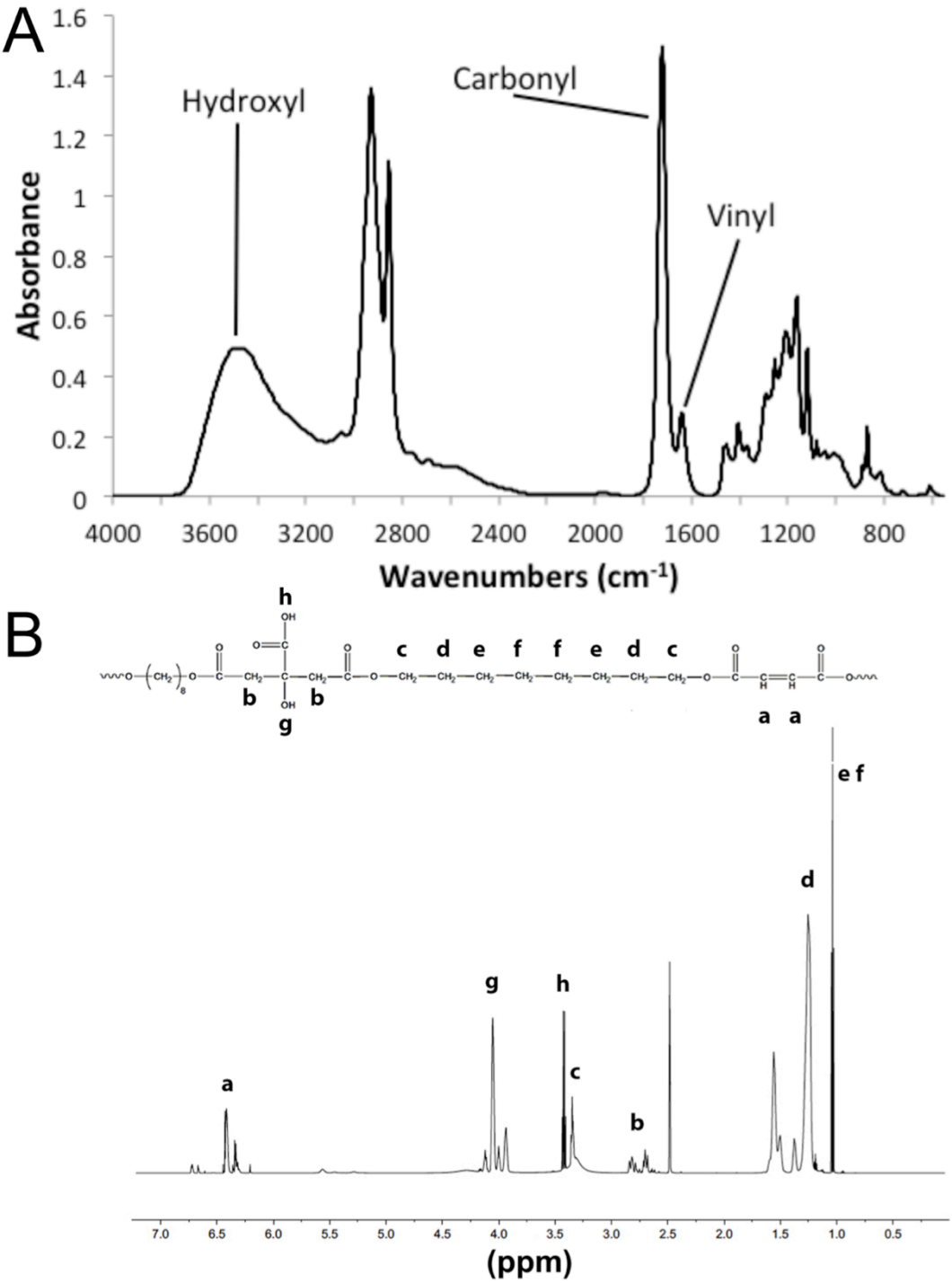

Supplementary Figure 2. Molecular structural characterization of POMaC pre-polymer.
(A) Fourier transform infrared (FT IR) spectroscopy. (B) Nuclear magnetic resonance (NMR) spectroscopy.

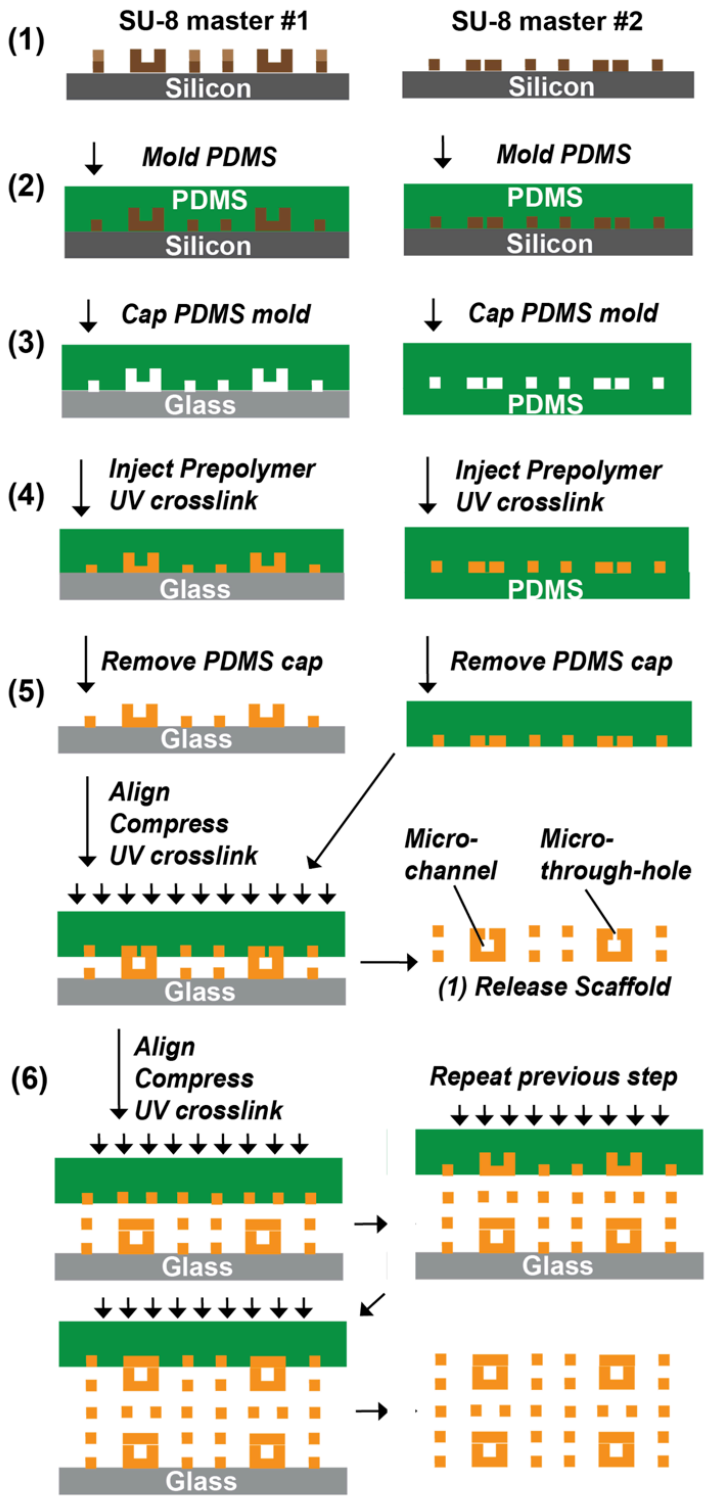

Supplementary Figure 3. Schematic of AngioChip scaffold micro-fabrication with 3-D stamping.
Each material is represented with a different color as following: SU-8 (brown), silicon wafer (black), PDMS (green), glass slide (grey), and POMaC (orange).

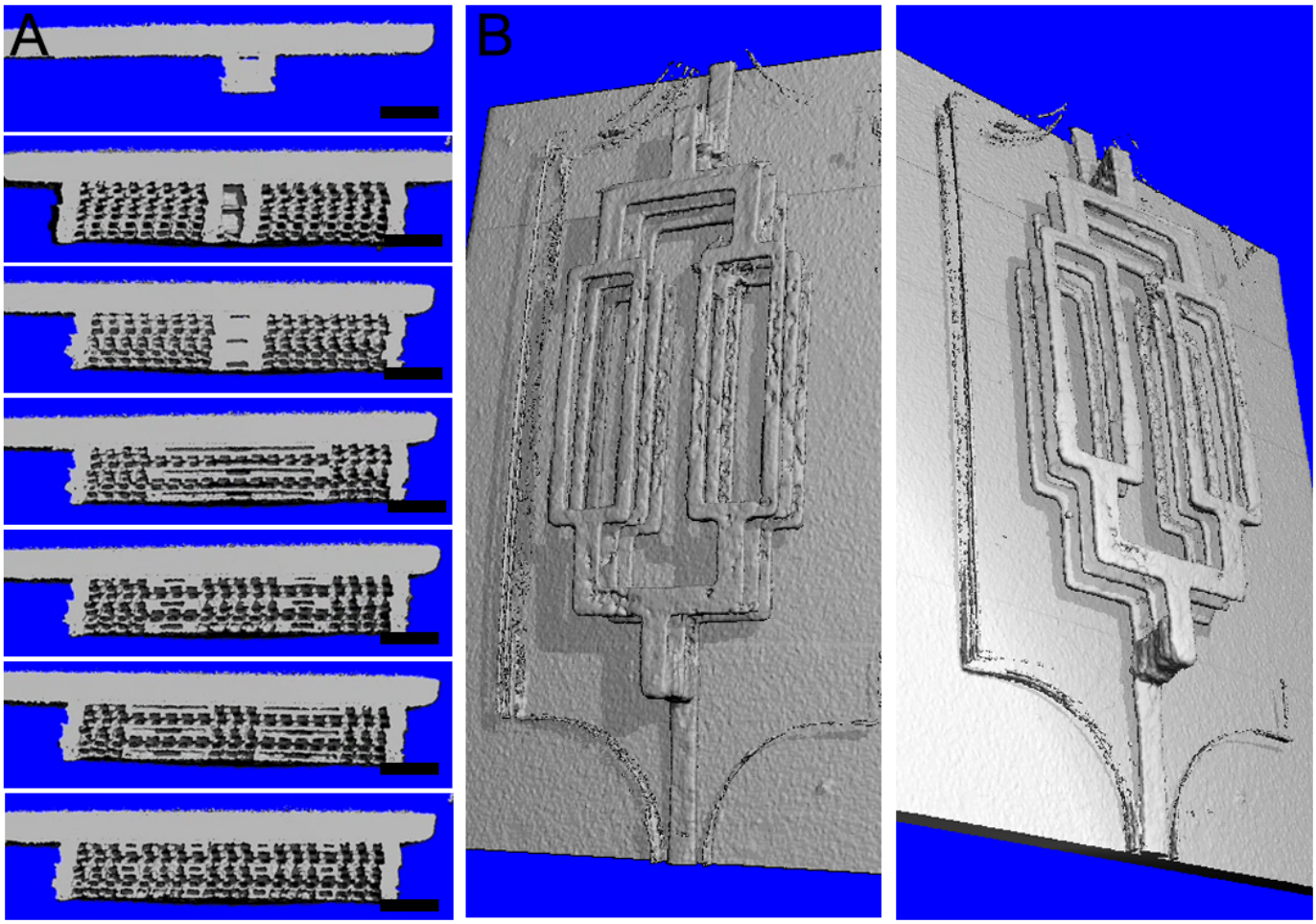

Supplementary Figure 4. Micro-computed tomography (MicroCT) of 3-D AngioChip scaffolds.
(A) MicroCT scans of the cross-section of a 3-D AngioChip scaffold from its inlet to the branches along the long-edge direction of the scaffold. Scale bar: 400µm. (B) MicroCT of the internal network of a 3-D AngioChip scaffold viewed from different angles. The scaffold was perfused with barium sulfate solution through its internal network hence increasing its density for improved visualization. The thickness of the scaffold network wall was 50µm. The inlet, outlet, and the first order branch had an inner luminal dimension of 50µm by 200µm. The second order branch had an inner luminal dimension of 50µm by 100µm. The network was designed so that the endothelial cells in the first and second order branches experienced the same level of shear stress. The networks on each layer were connected through a vertical channel and were 300µm apart in z-axis. The scaffold mesh was made of 50µm struts. The struts were spaced 250µm apart in the long-edge direction, 100µm apart in the short-edge direction, and 50µm apart in the z-axis. This version of the multi-layer scaffold has thickness of ~500µm.

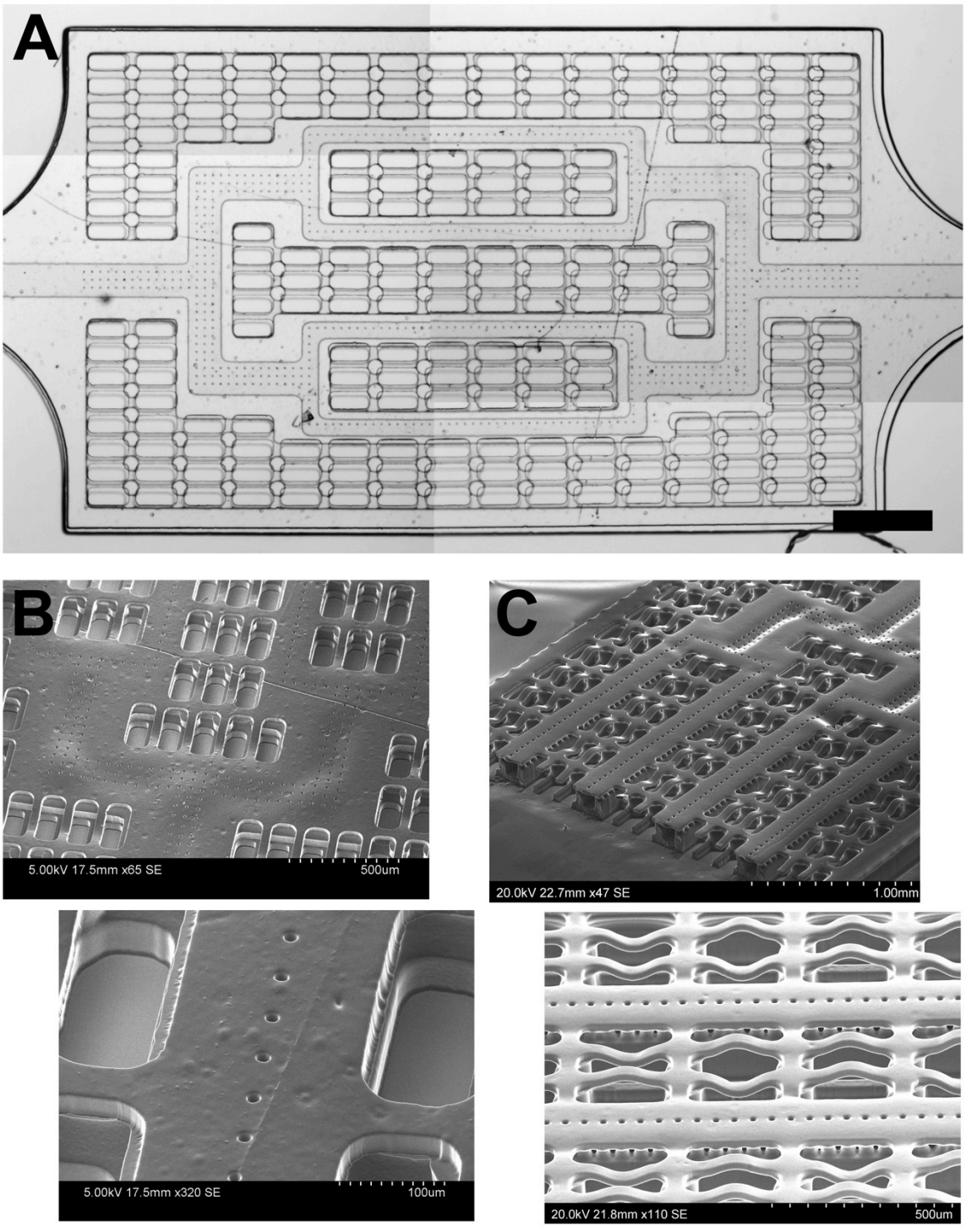

Supplementary Figure 5. AngioChip Scaffolds with micro-holes.
(A) Image of an AngioChip scaffold with 10µm micro-holes patterned throughout its network wall. Scale bar: 600µm. Image was stitched from multiple images. (B) SEM of an AngioChip scaffold with 10µm micro-holes viewed from different angles. Scale bars are shown in images. (C) SEM of an AngioChip scaffold with 20µm micro-holes on top and sidewalls viewed from different angles. Scale bars are shown in images.

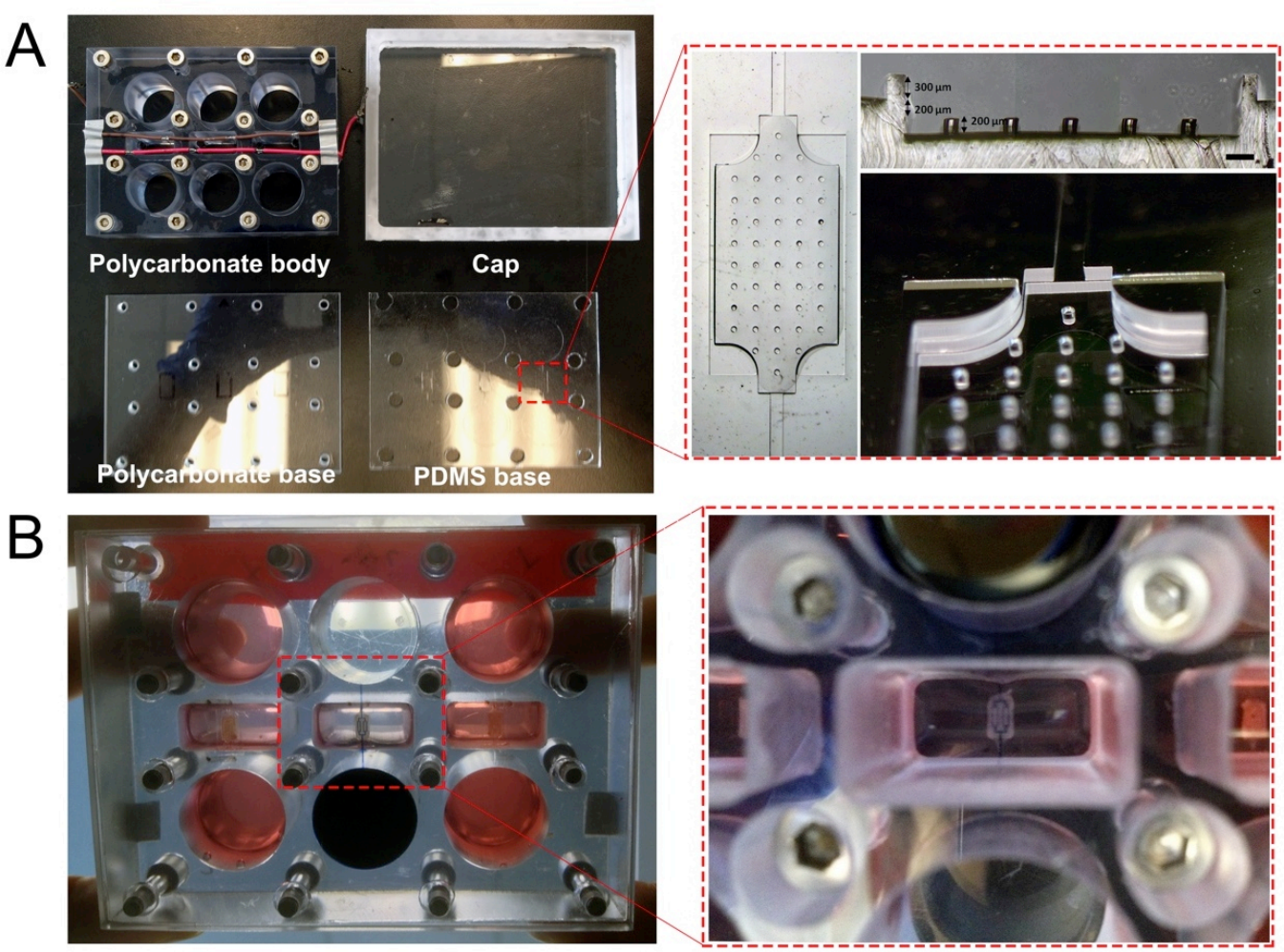

Supplementary Figure 6. Bioreactor assembly.
(A) Image of the four components (cap, polycarbonate body, PDMS base, and polycarbonate base) of the bioreactor. (Inset) Image of the trench structure on the PDMS base where the AngioChip scaffold was placed. An array of micro-posts was used to lift the AngioChip scaffold up ~200µm from the base so that cells could wrap around the scaffold from the bottom. The total height of the PDMS trench is 700µm. Cell/gel suspension was cast into the trench where the scaffolds were installed and filled to the top. (B) Image of the assembled bioreactor with three cardiac tissues perfused with color dye. (inset) Magnified image of a perfused cardiac tissue in the main well.

Parameter	AngioChip Scaffold			Rat Myocardium (n=4)
	Design A (n=3)	Design B (n=3)	Design C (n=3)	
E_{LD} (kPa)	89±22#	60±10*	22±6*#	43±9*
E_{SD} (kPa)	53±10#	31±4#	18±7	12±5
E_{LD}/E_{SD}	1.7±0.8#	2±0.6	1.4±0.6#	3.9±1.2
UTS_{LD}(kPa)	56±17	39±8	25±14	
UTS_{SD}(kPa)	22±8	15±3	8±4	
εf_{LD}(%)	70±18	69±17	96±45	
εf_{SD}(%)	54±17	61±22	45±5	

* Significantly different from corresponding sample tested in the short-edge direction.
# Significantly different from adult rat myocardium.

Supplementary Table 5. AngioChip mechanical properties.

Summary of the effective elasticity (E_{LD}, E_{SD}), anisotropic ratio (E_{LD}/E_{SD}), ultimate tensile stress (UTS_{LD}, UTS_{SD}) and strain-to-failure (εf_{LD} and εf_{SD}) measured in uniaxial direction for AngioChip scaffolds of different designs (average±s.d.). Corresponding properties for adult rat myocardium are shown for comparison. Long-edge direction (LD) and short-edge direction (SD) respectively corresponds to the circumferential and longitudinal axes of the heart.

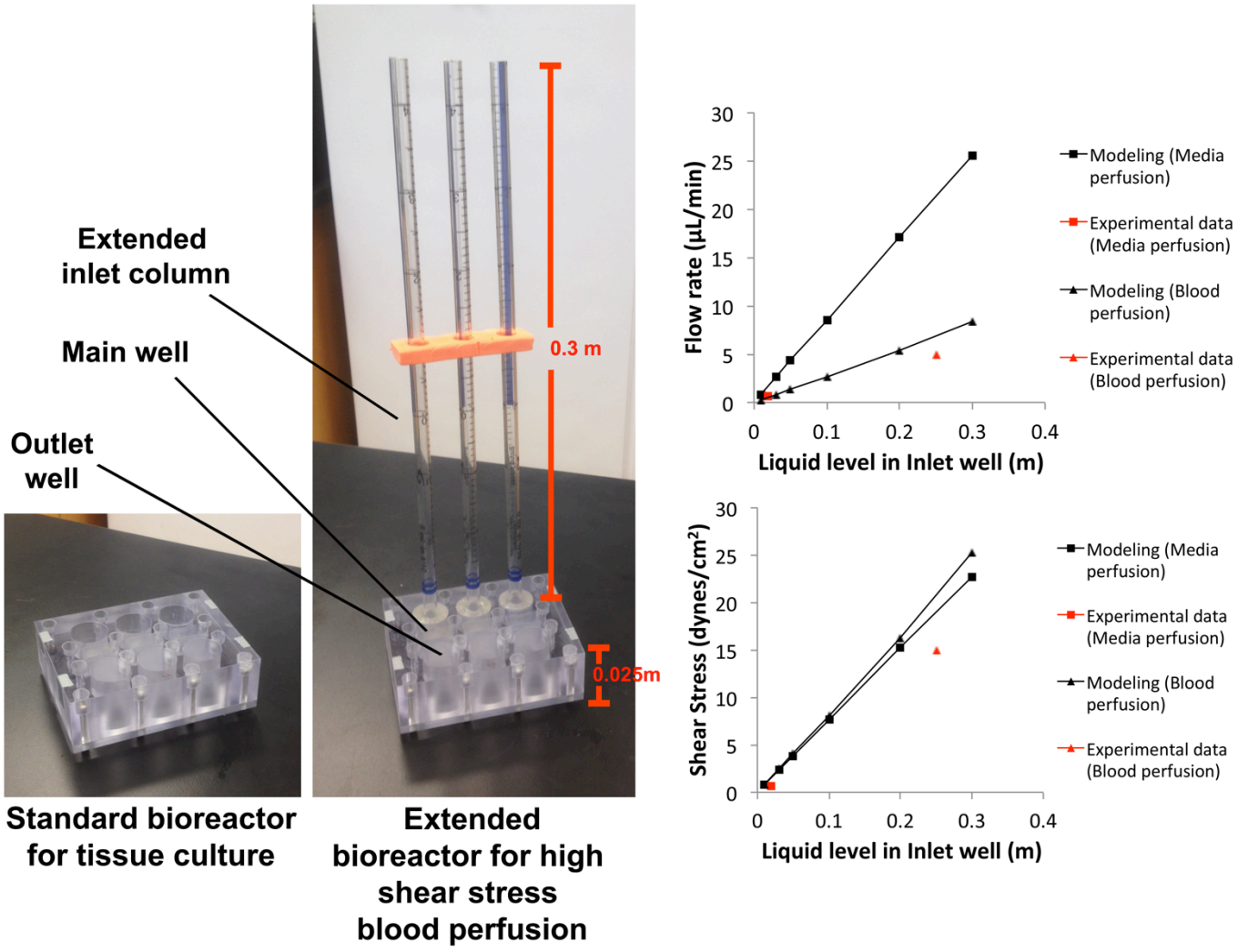

Supplementary Figure 7. Characterization of culture media and blood perfusion with the standard and the extended bioreactor setup.

To model the flow rate through the AngioChip scaffold with a given pressure head level, the pressure generated from a fluid column with a given height was first calculated based on the equation, $P = hg\rho$, where *P* stands for pressure, *h* stands for height, *g* is the gravitational constant, and ρ stands for density of the fluid. Then the inlet pressure head value was entered into COMSOL multi-physics where a geometrical model of the AngioChip network was created. Using the built-in Navier-Stokes equation, the volumetric flow rate through the network was then derived from the model. The wall shear stress was calculated from the derived volumetric flow rate based on the equation[18], $\tau = \frac{6\mu Q}{wH^2}$, where τ stands for shear stress, μ stands for viscosity, *w* and *H* stand for the width and height of the channel, and *Q* stands for the volumetric flow rate. The experimental volumetric flow rate was derived from the amount of fluid collected after one day of perfusion and the shear stress was derived from the corresponding volumetric flow rate.

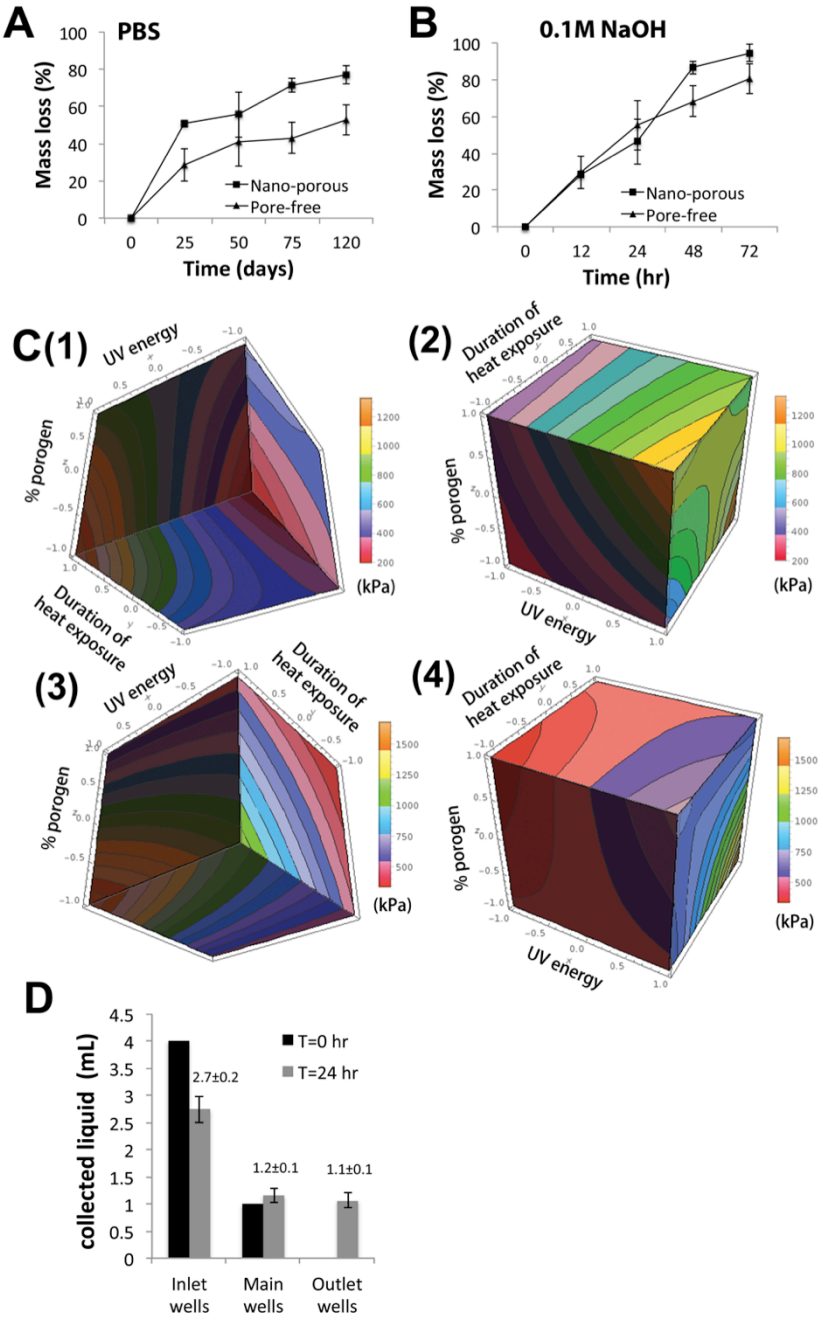

Supplementary Figure 8. AngioChip scaffold and polymer characterization.
Mass loss of AngioChip scaffolds with or without nano-pores in (A) PBS and (B) 0.1M NaOH solution (average±s.d., n=3). (C) Isosurface plot of the elasticity of the bulk POMaC polymer in relation to UV exposure energy, heat exposure duration, porogen content, and citric acid to maleic anhydride ratio. The cubes isosurface plots were rotated to show all 6 faces of the cube. Cube (1-2) shows conditions with low CA:MA ratio (0.25) and cube (3-4) shows conditions with high CA:MA ratio (1.5). 1.0, 0.0 and -1.0 correspond to the high, middle and low levels of the parameters named on the respective axis, as show for the design of experiment in **Supplementary Table 1** and **2**. (D) Measurement of volumetric perfusion of PBS through AngioChip scaffolds with 10µm micro-holes (average±s.d, n=4).

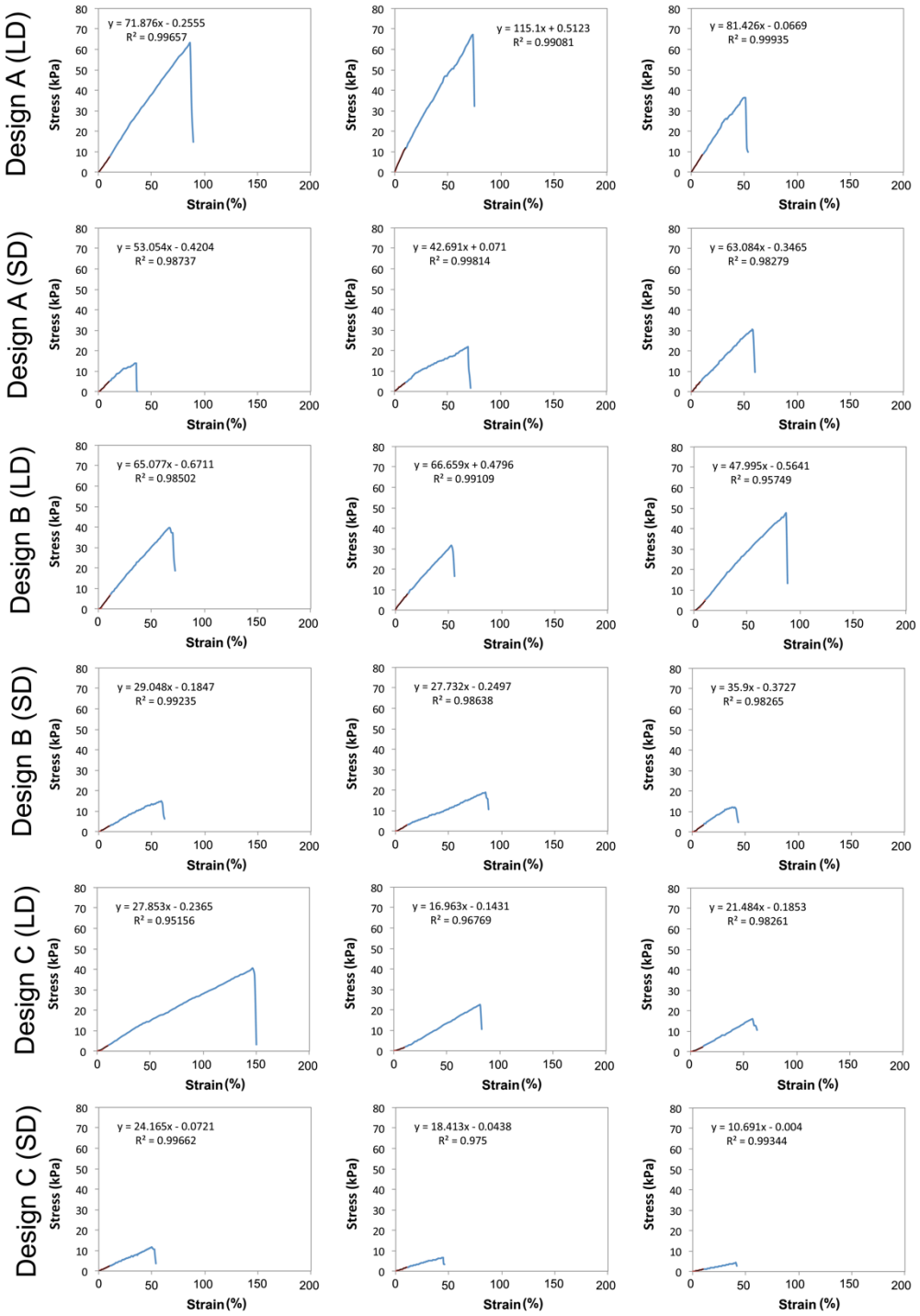

Supplementary Figure 9. Uniaxial tensile stress-strain plots of AngioChip scaffolds with the three different lattice designs.

The segments of the plots between strains of 0 to 10% were fitted with linear regression to calculate the effective stiffness (E). The Linear regression equations and the R-values are shown. The last data point before a significant drop in tensile stress was used to calculate the ultimate tensile stress (UTS) and the strain-to-failure (εf).

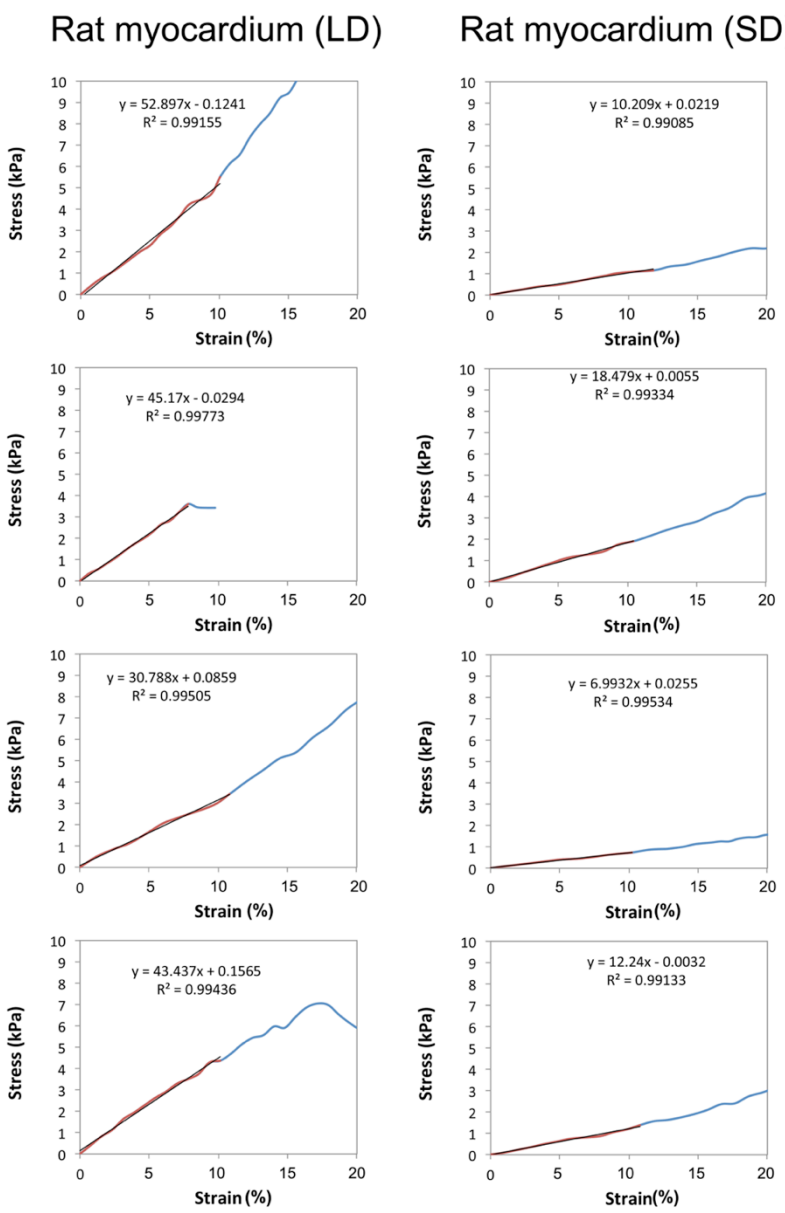

Supplementary Figure 10. Uniaxial tensile stress-strain plots of the adult rat ventricular myocardium. Long-edge direction (LD) and short-edge direction (SD) respectively corresponds to the circumferential and longitudinal axes of the heart. The segments of the plots between strains of 0 to 10% were fitted with linear regression to calculate the effective stiffness. The linear regression equations and the R-values are shown.

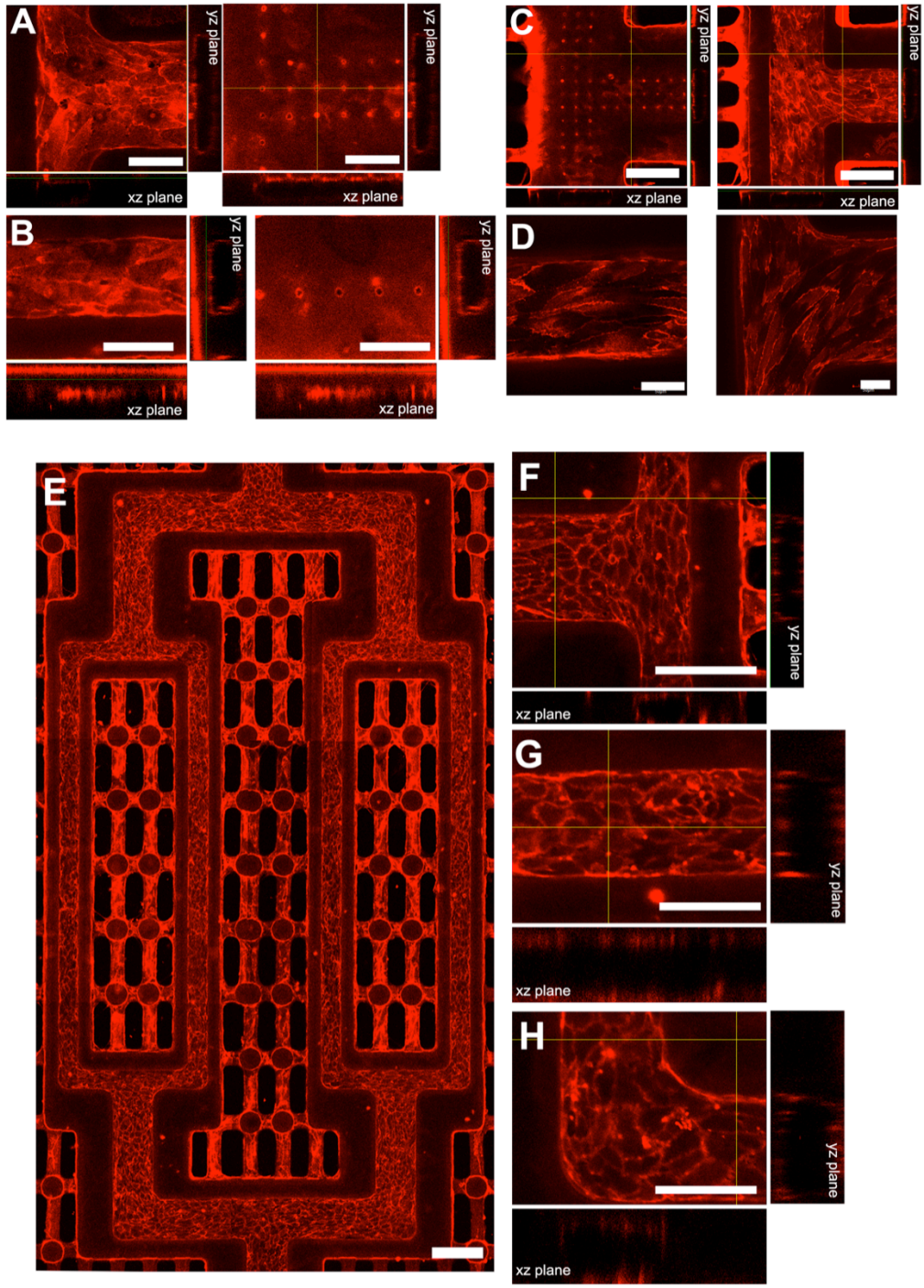

Supplementary Figure 11. Endothelialization of AngioChip scaffold network

(A-C, day 2) Confocal scan of HUVEC (CD31 immunostained, red) coverage on the scaffold network with 10µm micro-holes patterned on the network wall. Scale bar: (A) 100µm, (B) 100µm, (C) 200µm. (D) Confocal scan of the endothelial cell (VE-cadherin immunostained, red) coverage on the scaffold network. Scale bar: 50µm. (E-H, day 7) Immunostaining (CD31, red) of the internal vasculature of an Angiochip scaffold with 10µm micro-holes on day 7 with (E) a view of the entire network (scale bar: 200µm. Image was stitched from multiple images), (F) a view of a branch (scale bar: 200µm), (G) a straight segment (scale bar: 100µm), and (H) a corner (scale bar: 100µm).

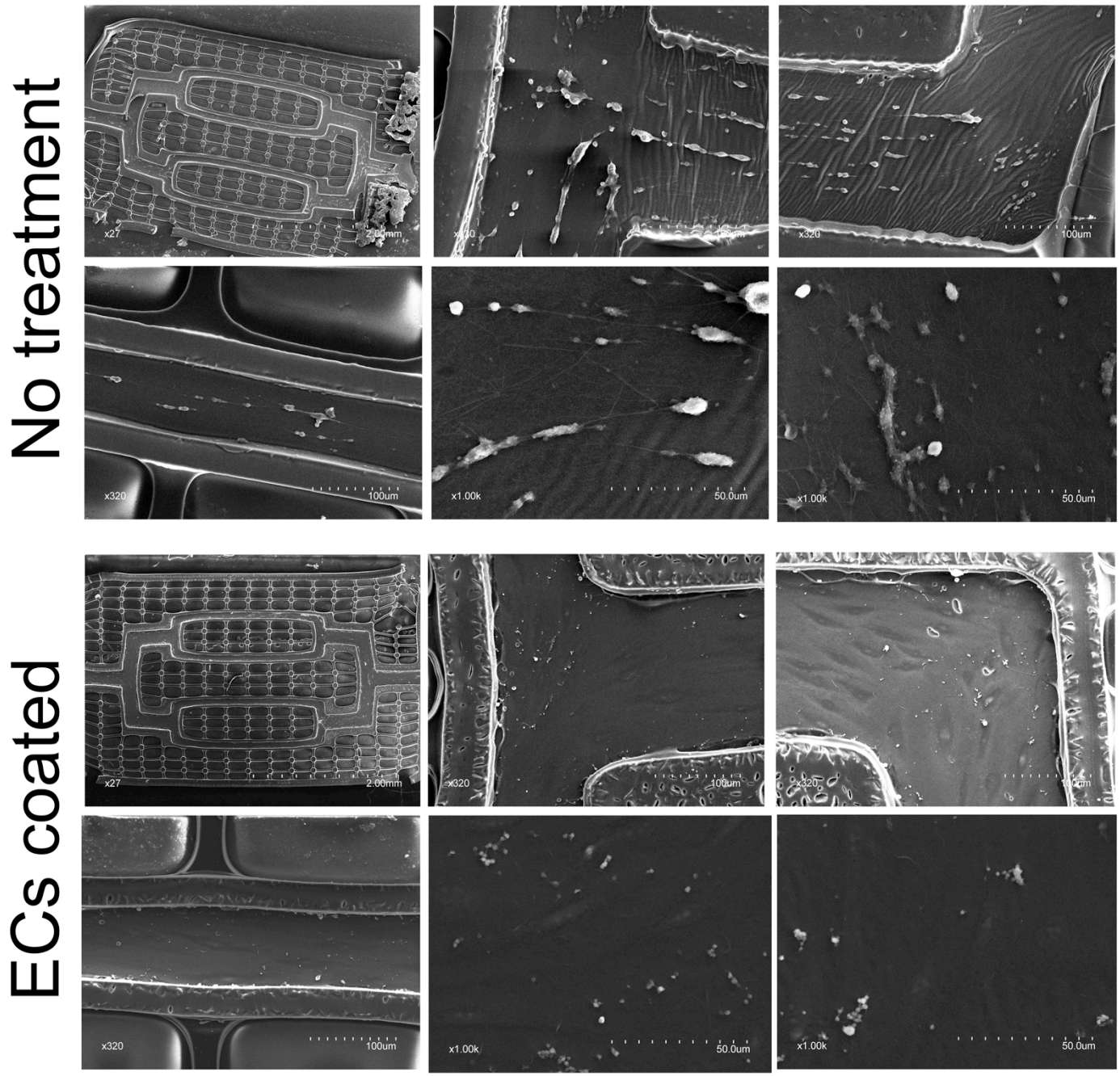

Supplementary Figure 12. AngioChip blood compatibility.
Representative SEM of the luminal surface of the AngioChip scaffold networks, with or without HUVEC coating (day 2 in culture), after the perfusion of human whole blood at 15dynes/cm^2 for 30min. Human blood was heparinized with 1% heparin (v/v) to prevent clotting during handling. Scale bars are shown in images.

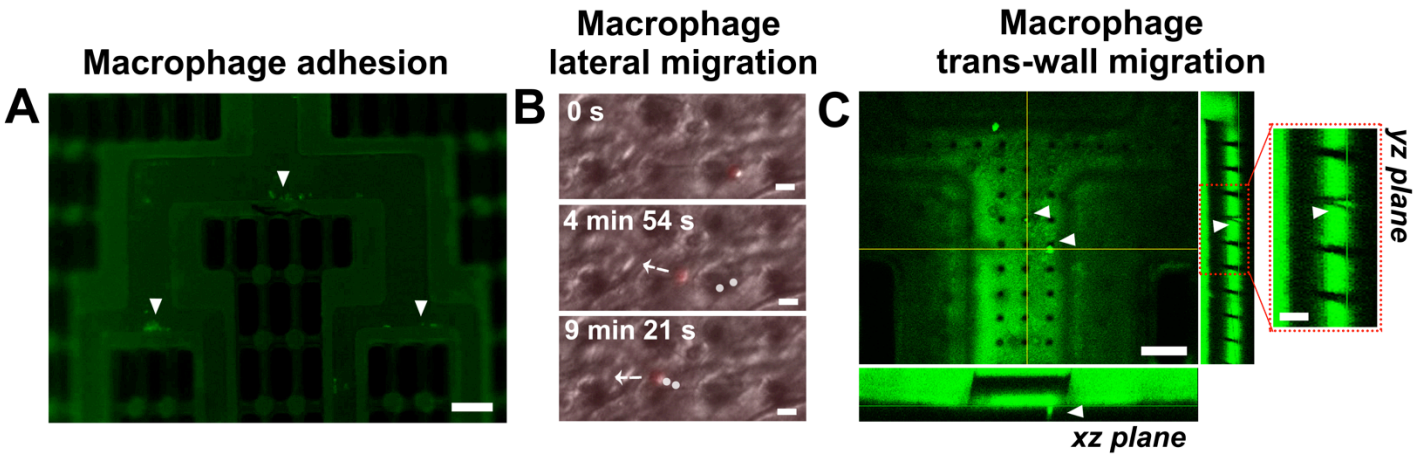

Supplementary Figure 13. Macrophage perfusion in endothelialized AngioChip.
(A) Fluorescent image showing adhesion and accumulation of fluorescently labeled RAW 267 cells (green) in the network branches (day 2 of culture). Scale bar: 200µm. White arrows indicate macrophage aggregates. (B) Time-lapse images of a fluorescently labeled macrophage (red) migrating laterally on the HUVEC-endothelialized surface of a scaffold network. Scale bar: 10µm. White arrows indicate the direction of macrophage migration. White dots indicate the position of the tracked cell in a previous captured frame. (C) Trans-wall migration of fluorescently labeled macrophages (green) through the 10µm micro-holes on the channel wall. Scale bar: 100µm. (Inset) scale bar: 50µm. White arrows indicate migrating macrophages.

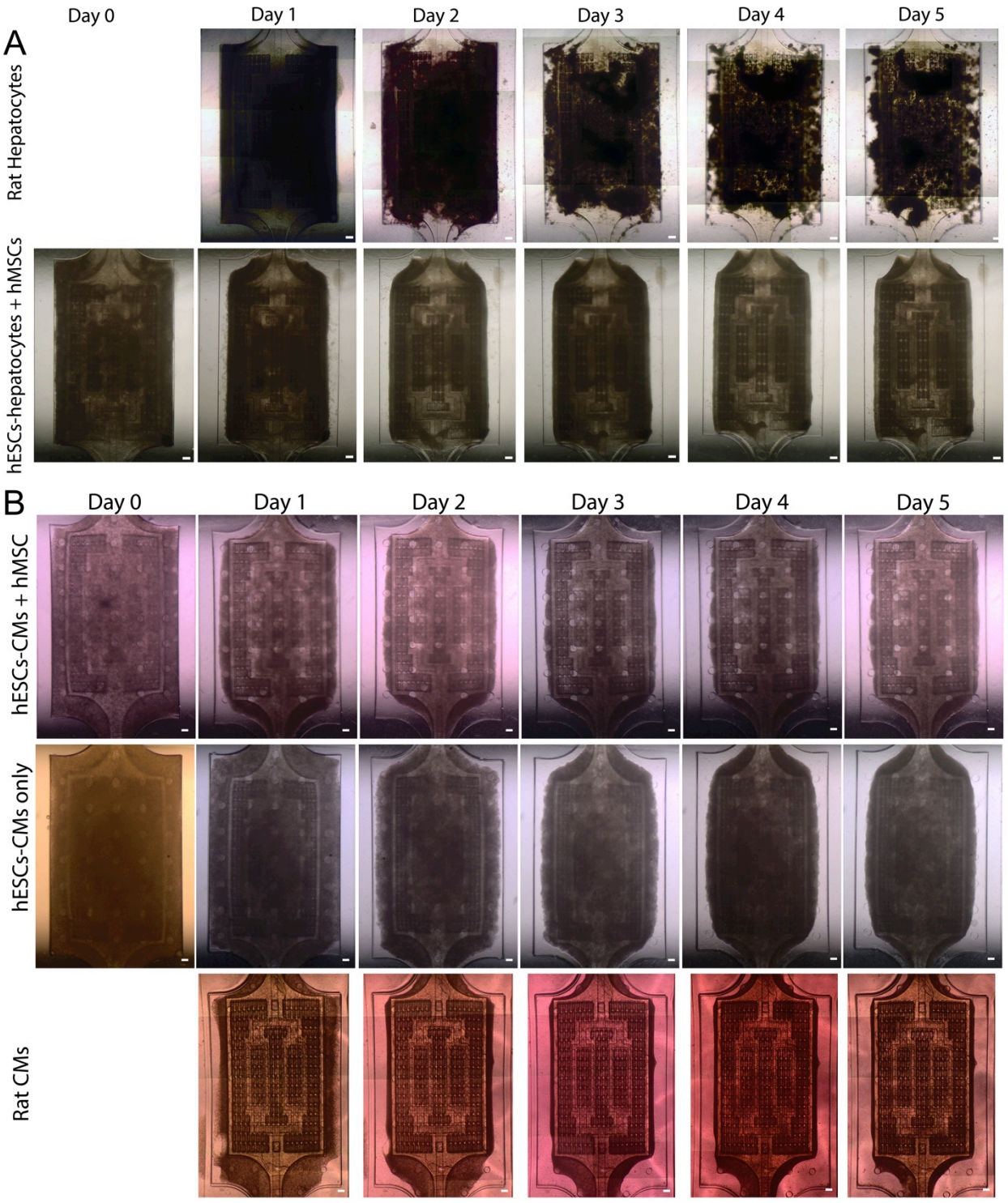

Supplementary Figure 14. Cell-gel compaction around AngioChip scaffold.

(A) Time-lapse of tissue remodelling over 5 days for rat hepatocytes or hESCs derived hepatocytes mixed with 20% hMSCs. Scale bar: 200µm. (B) Time-lapse of tissue remodelling over 5 days for hESCs derived cardiomyocytes with or witout 10% hMSCs or rat primary cardiomyocytes. Scale bar: 200µm.

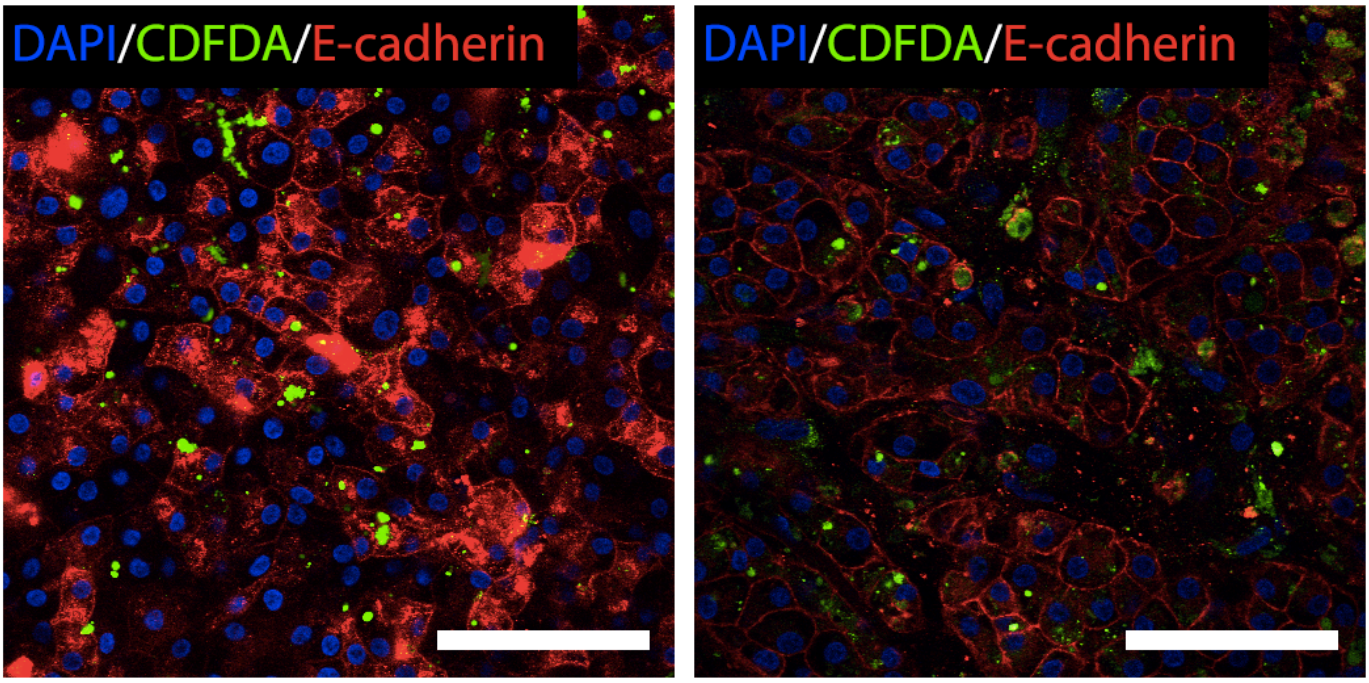

Supplementary Figure 15. Liver bile canaliculi.
Fluorescently labeled bile canaliculi with Carboxy-DCFDA on human hepatocyte monolayer in collagen sandwich (left) and human AngioChip hepatic tissue (right) on day 7. Scale bar: 100µm.

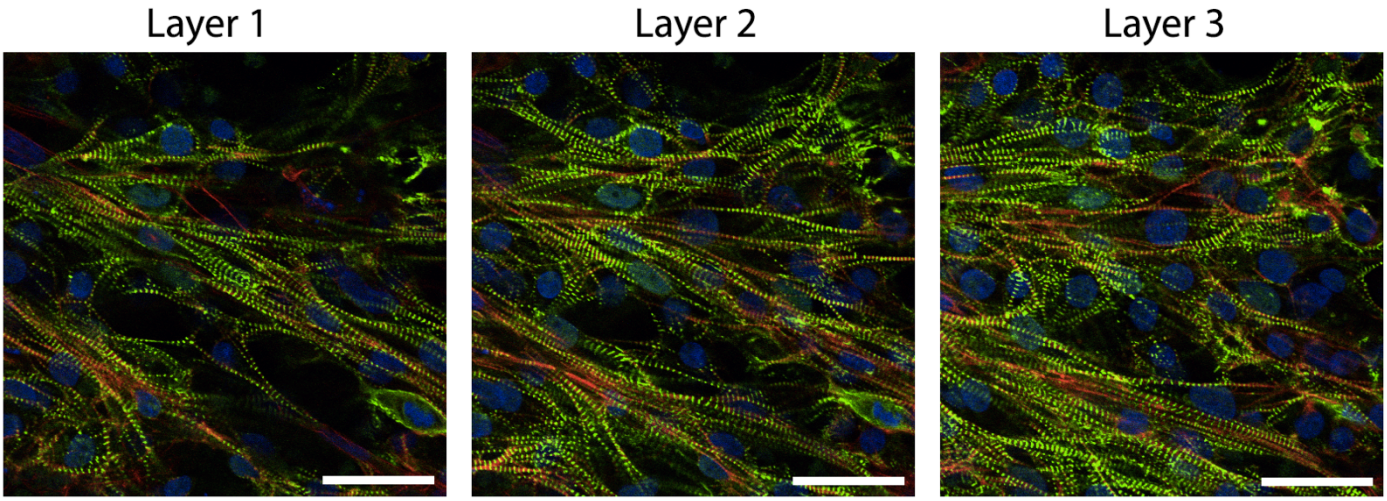

Supplementary Figure 16. Human cardiomyocyte morphology on AngioChip
Confocal z-stack of a section of a human AngioChip cardiac tissue based on hESC-derived cardiomyocytes and 10% MSCs, shows cardiomyocytes overlapping each other forming bundle-like structures. Tissue stained for sarcomeric α-actinin (green), F-actin (red), and DAPI (blue). Scale bar: 40µm. Distance between each layer is 2µm.

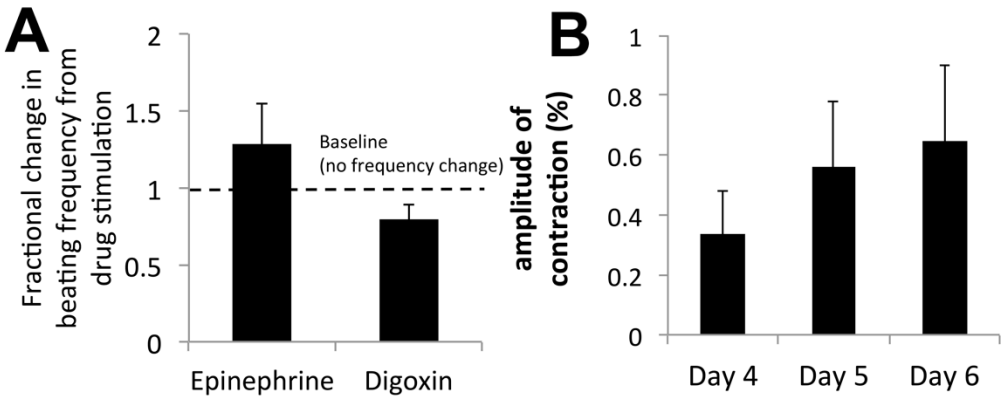

Supplementary Figure 17. AngioChip cardiac tissue.

(A) Response of human AngioChip cardiac tissue with 10μm micro-holes to perfused cardiac drugs (10μM Epinephrine, n=3 and 10μM Digoxin, n=4, average ± s.d.) on day 7. AngioChip displayed expected positive chronotropic response to epinephrine and negative chronotropic response to digoxin at concentration of 10μM as shown previously[19]. (B) The percent amplitude of contraction of the human cardiac tissues between day 4-6 (average±s.e.m., n=4).

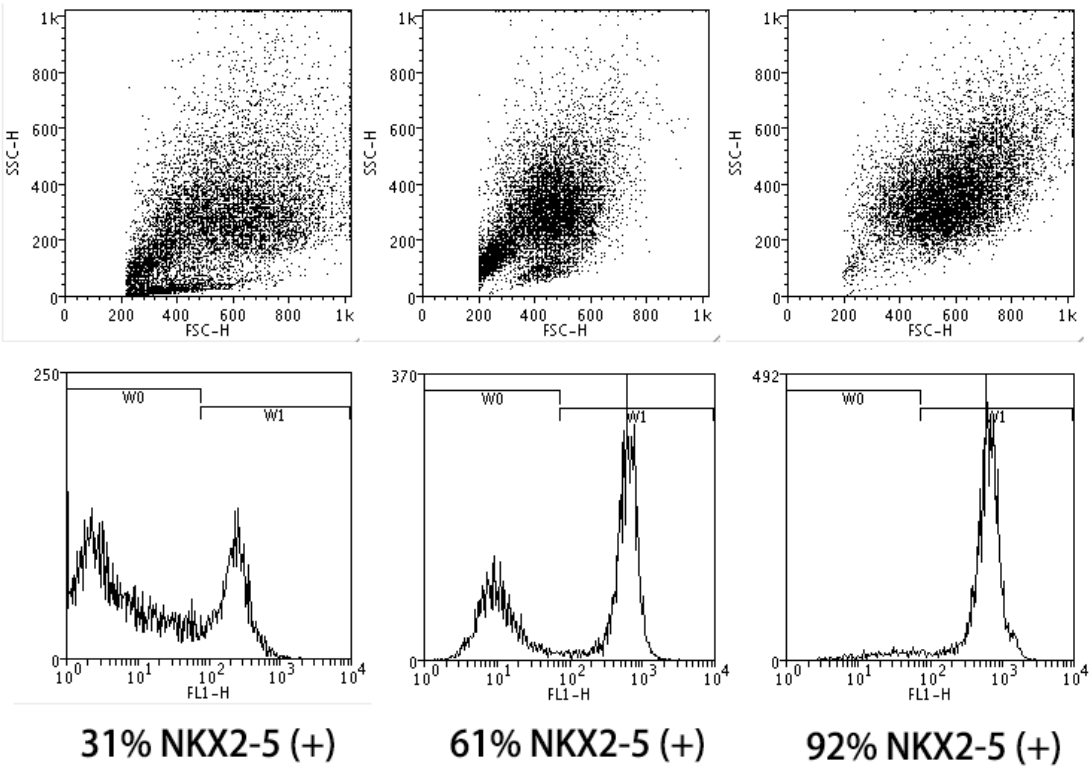

Supplementary Figure 18. Flow cytometry analysis of HES-3 NKX2-5 GFP positive cells.

Representative data on low purity, median purity, and high purity cardiomyocytes obtained from differentiation. FL1-H corresponds to NKX2-5 expression. NKX2-5 positive cells were considered to be cardiomyocytes. Percent of cardiomyocytes in each cell mixture were determined by the W1 gated region. The average purity of cardiomyocytes was 51±23% over the course of the experiments.

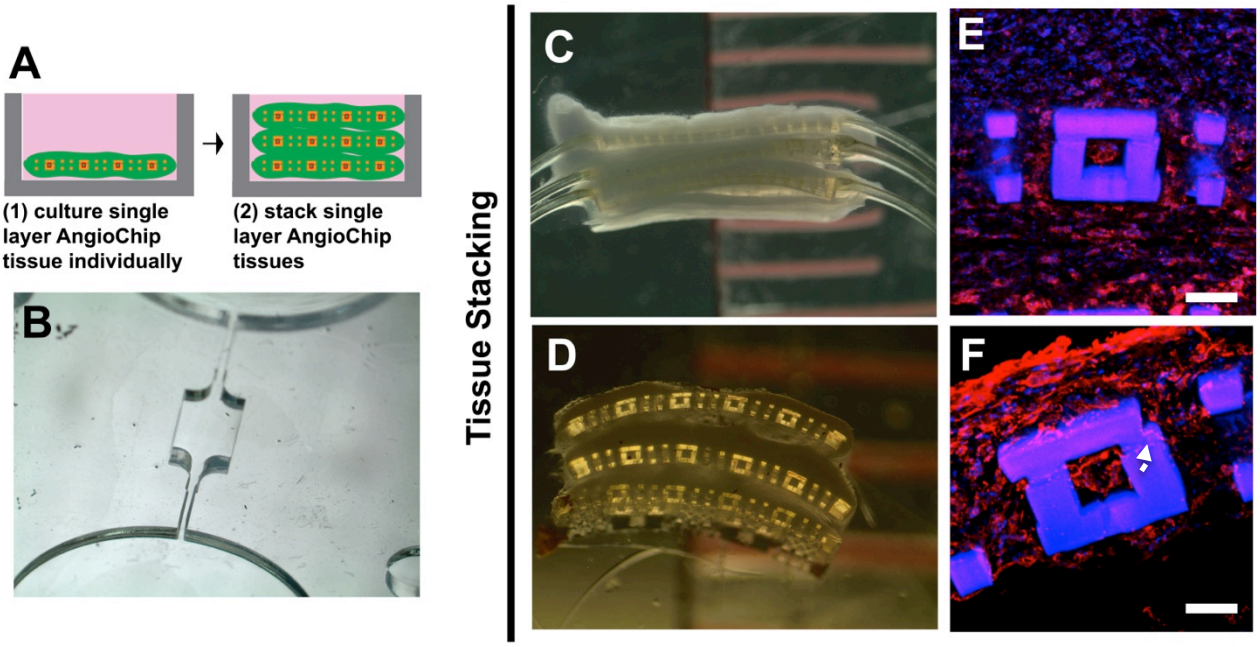

Supplementary Figure 19. Milimeter-scale thick tissue assembly by stacking of individual single-layer AngioChip tissues based on human cells.

(A) Schematic of the thick tissue assembly process based on tissue stacking method. (B) Image of a tissue chamber with a greater depth (~1.5mm) for stacking of multiple tissues. (C,D) Image of a 2mm thick AngioChip cardiac tissue with 20μm micro-holes cultivated for 3 days stacked from 3 single layer AngioChip cardiac tissues with (C) a side view and (D) a cross-sectional view (n=3). Scale shown in mm. (E,F) Immunostaining of CD31 (red) on the cross-section of an endothelialized engineered vessel in the thick tissue. Endothelial sprouting (arrow) is visible from the 20μm micro-holes on the channel sidewalls. Scale bar: (E) 100μm (F) 50μm.

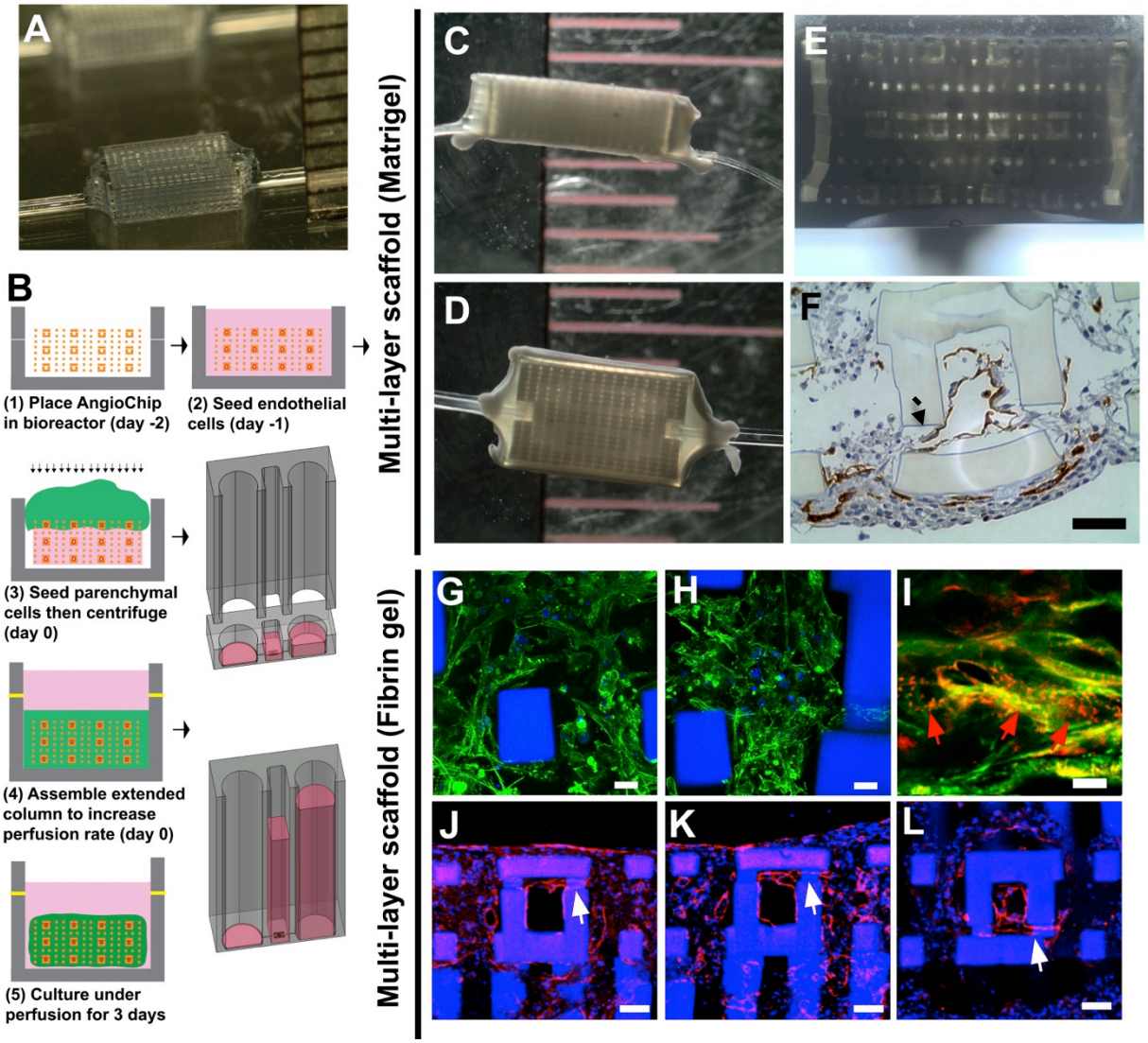

Supplementary Figure 20. Engineering of millimeter-scale tissues using multi-layer AngioChip scaffolds with single inlet and single outlet.

(A) Image of a thick AngioChip scaffold (1.58mm) with a built-in multi-layer channel network with 20μm micro-holes perfusable from a single inlet and outlet. Scale shown in mm. (B) Schematic of the thick tissue assembly process based on centrifugation-facilitated cell seeding of the thick multi-layer AngioChip scaffold with a single inlet and single outlet. (C-E) Image of a thick AngioChip cardiac tissue based on human cells seeded with Matrigel and cultured for 3 days; (C) side view, (D) top view, and (E) cross-sectional view. Scale shown in mm. (F) Histology section of CD31 (brown) on an endothelialized engineered vessel in the thick tissue. Scale bar: 50μm. Endothelial sprouting is visible from the micro-holes on the channel side walls (arrow). (G,H) Immunostaining of F-actin (green) from the center of the cross-section of a thick human cardiac AngioChip tissue on day 3. Scale bar: 20μm. (I) High magnification image (F-actin: green, and sarcomeric-α-actinin: red) from the center of the cardiac tissue cross-section. Red arrow points to cross-striations. Scale bar: 5μm. (J-L) Immunostaining of CD31 on the cross-section of endothelialized thick human AngioChip cardiac tissues on day 3 zoom-in at (J,K) the edge of the tissues and (L) the center of the tissues. White arrow points to endothelial cells sprouting from the main AngioChip lumen into the parenchymal space. Scale bar: 50μm

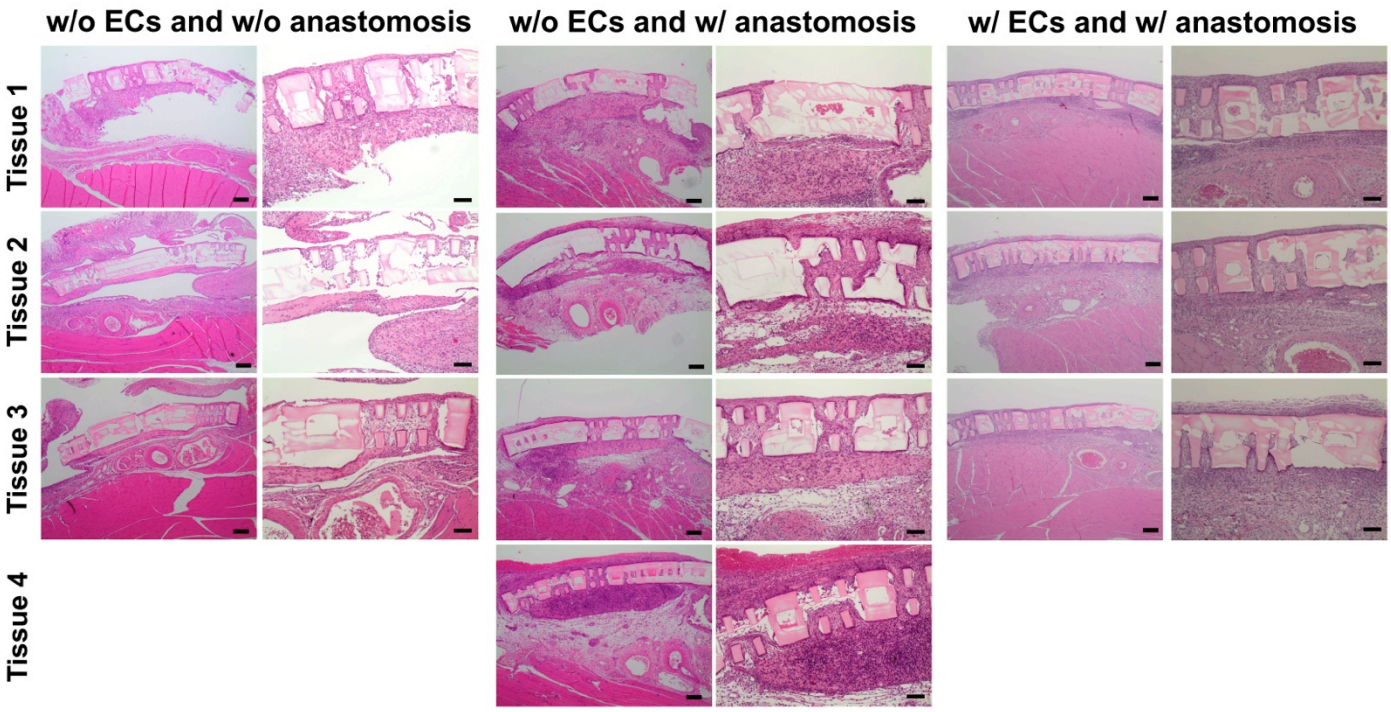

Supplementary Figure 21. H&E staining of AngioChip tissue implants.

H&E stained histology cross-section of the non-endothelialized or endothelialized cardiac tissue implants after 1 week with or without the direct surgical anastomosis in the configuration of artery-to-vein graft. Scale bar in column 1,3,5: 200µm. Scale bar in column 2,4,6: 100µm

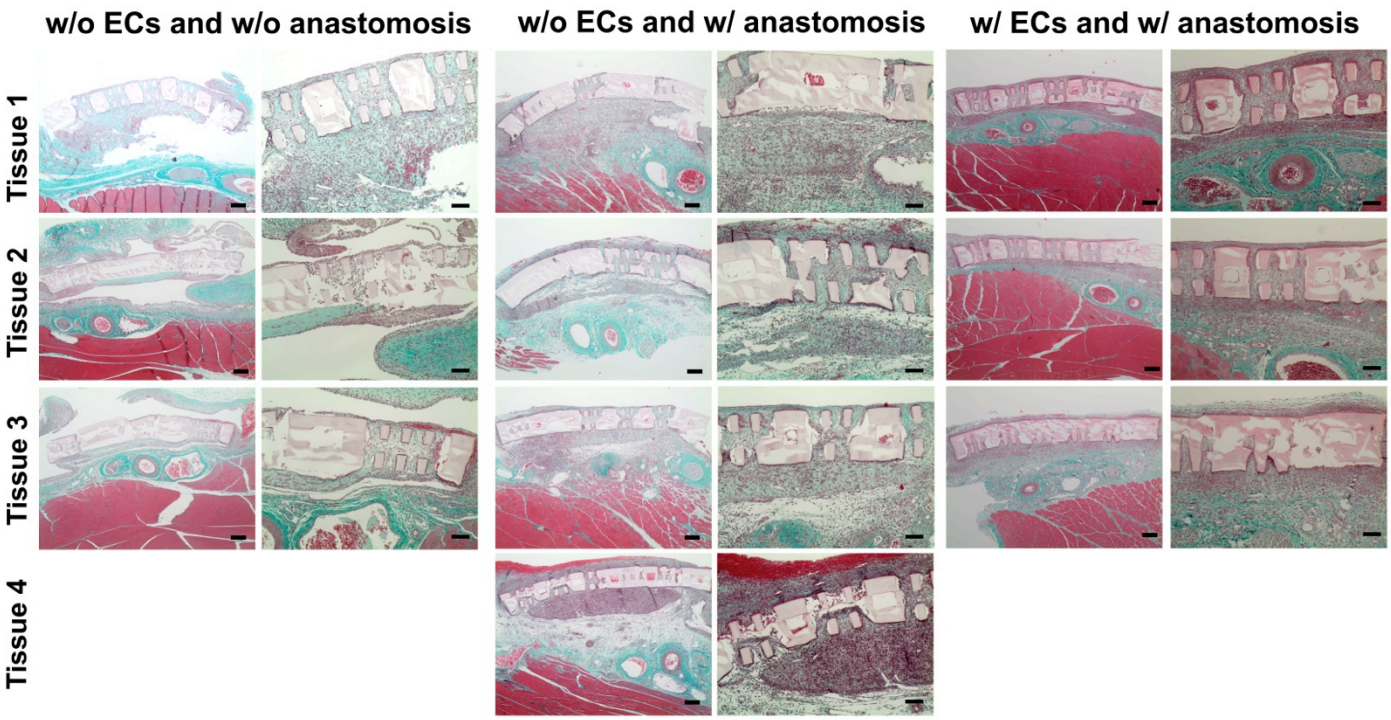

Supplementary Figure 22. Masson's trichrome staining of AngioChip tissue implants.
Masson's trichrome stained histology cross-section of non-endothelialized or endothelialized the cardiac tissue implants after 1 week with or without the direct surgical anastomosis in the configuration of artery-to-vein graft. Scale bar in column 1,3,5: 200µm. Scale bar in column 2,4,6: 100µm.

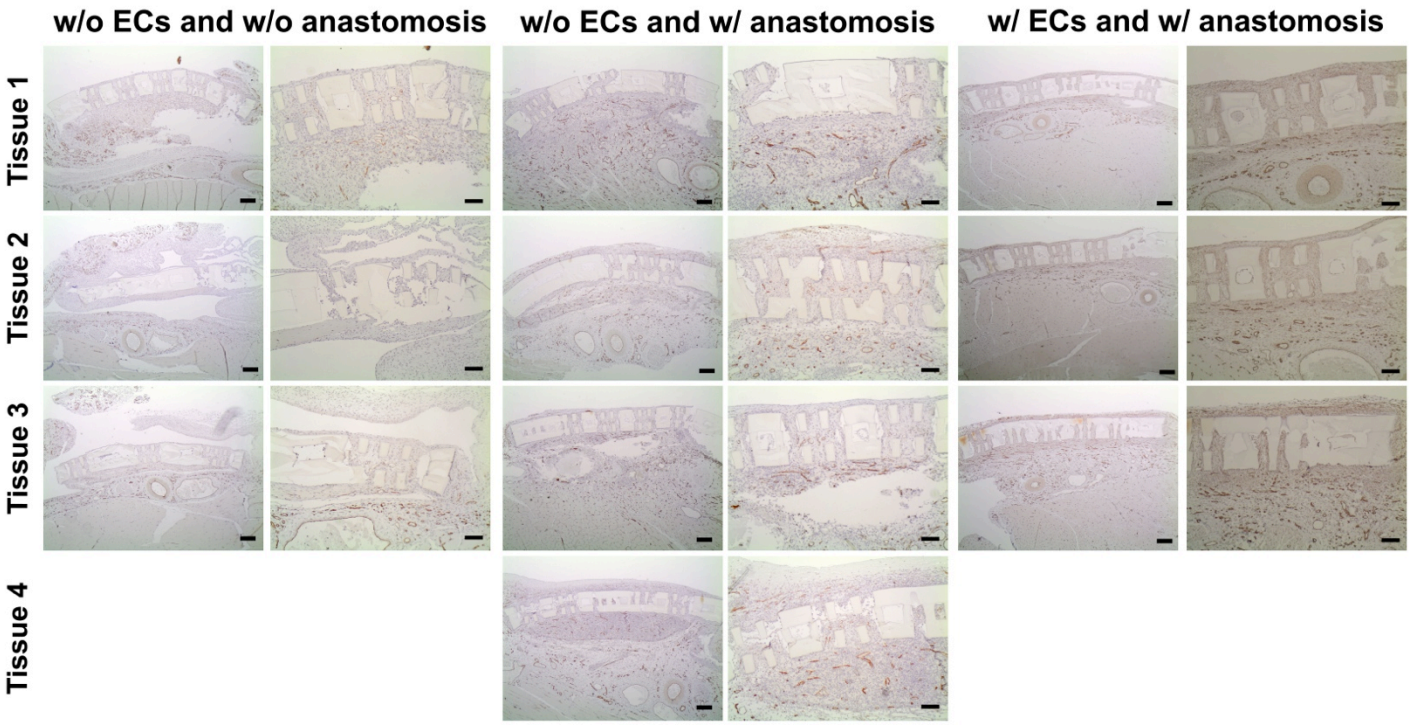

Supplementary Figure 23. CD31 staining of AngioChip tissue implants.

CD31 stained histology cross-section of the non-endothelialized or endothelialized cardiac tissue implants after 1 week with or without the direct surgical anastomosis in the configuration of artery-to-vein graft. Scale bar in column 1,3,5: 200µm. Scale bar in column 2,4,6: 100µm.

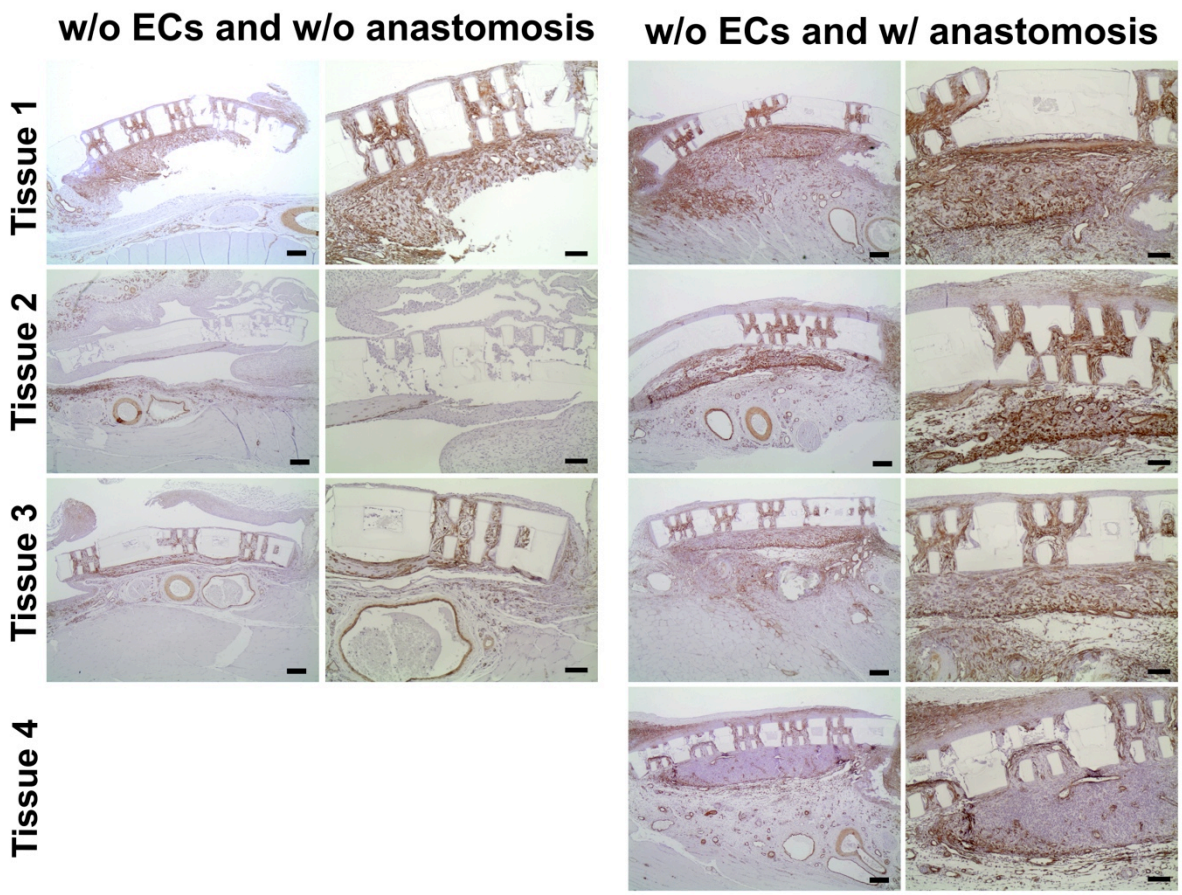

Supplementary Figure 24. Smooth muscle actin staining of AngioChip tissue implants.
Smooth muscle actin (SMA) stained histology cross-section of the cardiac tissue implants after 1 week with or without the direct surgical anastomosis in the configuration of artery-to-vein graft. Scale bar in column 1,3: 200µm. Scale bar in column 2,4: 100µm.

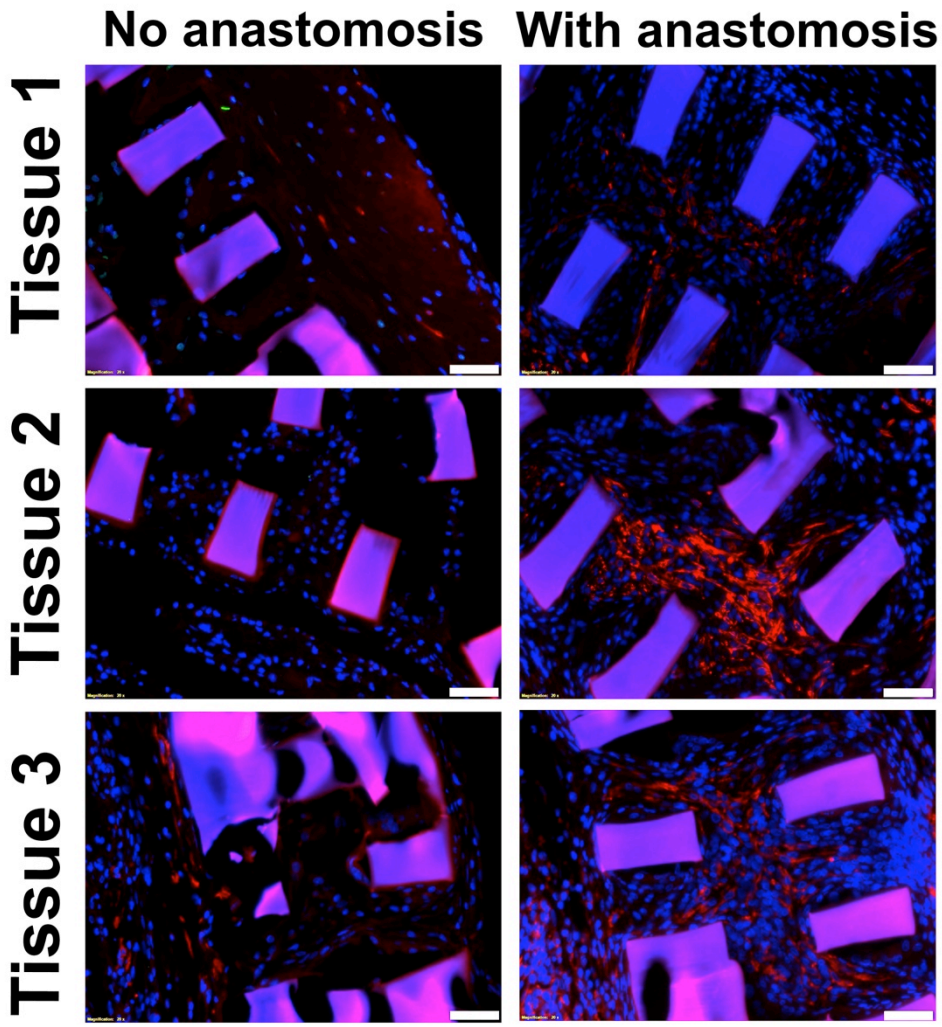

Supplementary Figure 25. Cardiac Troponin T staining AngioChip tissue implants.
Immunostaining of the cross-section of the cardiac tissue implants after 1 week with or without the direct surgical anastomosis in the configuration of artery-to-vein graft. Troponin T (red), DAPI (blue). Scale bar: 50µm.

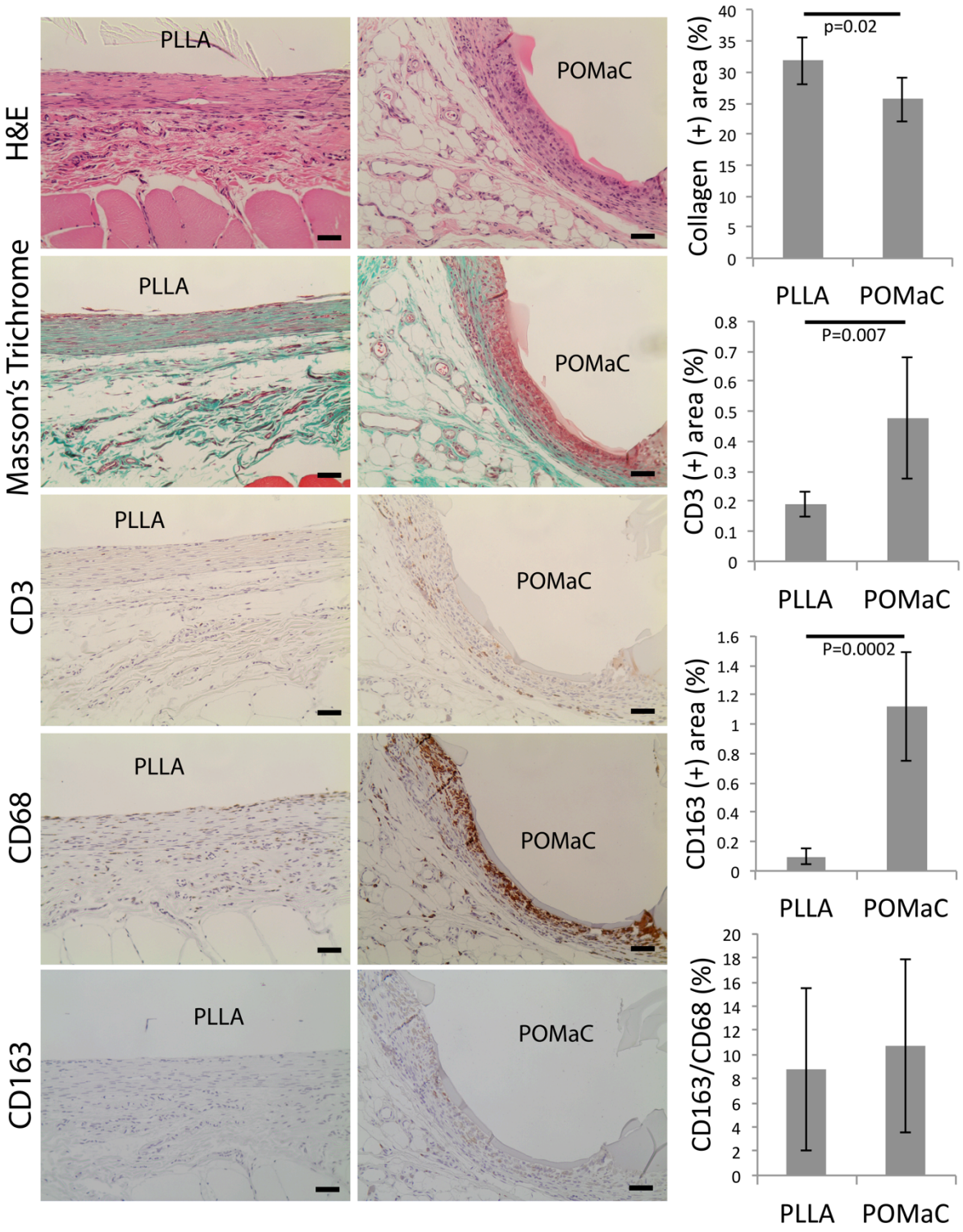

Supplementary Figure 26. Biocompatibility in vivo.

Histology cross-sections of the native tissue and implanted PLLA or POMaC disk interface after 5 weeks of subcutaneous implantation in an adult Lewis rat. The sections were stained with H&E, Masson's Trichrome, CD3, CD68, and CD163. Scale bar: 50µm. Quantification of stained area within 200µm (400pixels) distance from the tissue and implant interface (average±s.d, n=6).

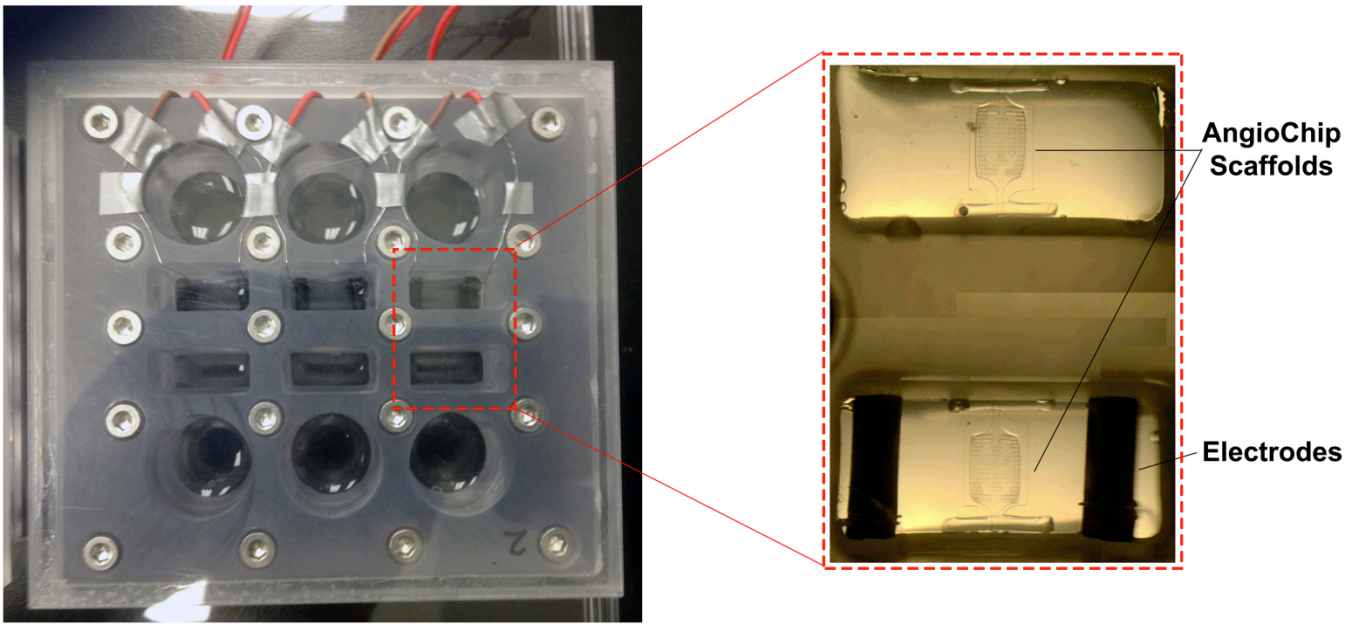

Supplementary Figure 27. Towards human-on-a-Chip, strategic compartment integration.
Image of a dual-well bioreactor where two main wells were included between each inlet well and outlet well. Two AngioChip scaffolds can be connected in series and perfused sequentially from the inlet well to the outlet well. (inset) Magnified image of the dual-well where two AngioChip scaffolds were installed. Hepatocytes can be seeded onto the first scaffold while cardiomyocytes can be seeded onto the second scaffold to create an "organ-on-a-chip" system for probing organ level drug interaction. A pair of electrodes was installed in the second chamber for stimulating cardiac tissues.

Supplementary Videos

Supplementary Movie 1. MicroCT scan and perfusion of a 3-D AngioChip scaffold. A 3-D AngioChip scaffold was scanned from its inlet to its outlet with a microCT. The cross-sections are revealed. The red vertical line indicates the location of the cross-section along the long-edge of the scaffold. To show the built-in network of the scaffold is perfusable, the network was perfused with color dye. The branched network on all three layers was perfused sequentially.

Supplementary Movie 2. Controlled dilation of the AngioChip network.

Supplementary Movie 3. Confocal scan of a multi-layer endothelialized AngioChip network with CD31 immunostaining. CD31: red. The first branch of the multi-layer AngioChip network is shown. A vertical channel was used to connect the branched networks on different levels. Endothelial cells are shown to coat the inner luminal surface of the multi-layer network.

Supplementary Movie 4. Contraction and perfusion of an AngioChip cardiac tissue. At day 7, an AngioChip cardiac tissue spontaneously contracts by bending the scaffold structure. The bending is more pronounced on the left and right edge since the top and bottom edge of the tissue were anchored to the bioreactor to allow perfusion. To show perfusion, the tissue was then perfused with color dye. The play speed was accelerated 10 times to show the progression of color change in the network. The total perfusion time is ~2 min.

Supplementary Movie 5. Cardiac AngioChip contraction before and after removal from the bioreactor, day 7 in culture.

Supplementary Movie 6. Conduction velocity activation map in a human AngioChip cardiac tissue. The point of the stimulation is on the right side. The color change through the tissue indicates the impulse propagation from the point of stimulation.

Supplementary Movie 7. Initiation of immediate blood perfusion through implanted AngioChips with surgical vascular anastomosis on the femoral vessels of rat hindlimb. Two surgical configurations were demonstrated. One configuration is artery bypass where the inlet and outlet of the AngioChip network were both connected to an artery. The blood from the femoral artery was routed through the AngioChip and back to the artery. Another is artery to vein loop where the inlet of the AngioChip network was connected to an artery while the outlet was connected to a vein. The blood from the femoral artery was routed through the AngioChip and delivered directly to the femoral vein, going back to the heart. Surgical vessel clamps were used to shut the artery and vein temporarily during surgery. After the surgical procedure, vessel clamps were removed and blood was perfused immediately through the AngioChip network in both surgical configurations. Vessel pulsation can also be observed on the AngioChip network.

References

1 Engelmayr, G. C. *et al.* Accordion-like honeycombs for tissue engineering of cardiac anisotropy. *Nature Materials* **7**, 1003-1010, doi:10.1038/nmat2316 (2008).

2 Rappaport, D., Adam, D., Lysyansky, P. & Riesner, S. Assessment of myocardial regional strain and strain rate by tissue tracking in B-mode echocardiograms. *Ultrasound in Medicine & Biology* **32**, 1181-1192 (2006).

3 Patel, S. V., McLaren, J. W., Camp, J. J., Nelson, L. R. & Bourne, W. M. Automated quantification of keratocyte density by using confocal microscopy in vivo. *Investigative ophthalmology & visual science* **40**, 320-326 (1999).

4 Zhang, B., Montgomery, M., Davenport-Huyer, L., Korolj, A. & Radisic, M. Platform technology for scalable assembly of instantaneously functional mosaic tissues. *Science Advances* **1**, doi:10.1126/sciadv.1500423 (2015).

5 Nunes, S. S. *et al.* Biowire: a platform for maturation of human pluripotent stem cell-derived cardiomyocytes. *Nature methods* **10**, 781-787 (2013).

6 Takahashi, R., Sonoda, H., Tabata, Y. & Hisada, A. Formation of Hepatocyte Spheroids with Structural Polarity and Functional Bile Canaliculi Using Nanopillar Sheets. *Tissue Engineering Part A* **16**, 1983-1995, doi:10.1089/ten.tea.2009.0662 (2010).

7 Tran, R. T. *et al.* Synthesis and characterization of a biodegradable elastomer featuring a dual crosslinking mechanism. *Soft Matter* **6**, 2449-2461, doi:10.1039/C001605E (2010).

8 Kibbe, M. R. *et al.* Citric acid-based elastomers provide a biocompatible interface for vascular grafts. *Journal of Biomedical Materials Research Part A* **93A**, 314-324, doi:10.1002/jbm.a.32537 (2010).

9 Motlagh, D. *et al.* Hemocompatibility evaluation of poly(diol citrate) in vitro for vascular tissue engineering. *Journal of Biomedical Materials Research Part A* **82A**, 907-916, doi:10.1002/jbm.a.31211 (2007).

10 Spiller, K., Freytes, D. & Vunjak-Novakovic, G. Macrophages Modulate Engineered Human Tissues for Enhanced Vascularization and Healing. *Annals of Biomedical Engineering*, 1-12, doi:10.1007/s10439-014-1156-8 (2014).

11 Seifert, B., Groth, T., Herrmann, K. & Romaniuk, P. Immobilization of heparin on polylactide for application to degradable biomaterials in contact with blood. *Journal of Biomaterials Science, Polymer Edition* **7**, 277-287 (1996).

12 Welty, J. R., Wicks, C. E., Rorrer, G. & Wilson, R. E. *Fundamentals of momentum, heat, and mass transfer*. Fifth edn, 497-500 (John Wiley & Sons, 2007).

13 Periasamy, N. & Verkman, A. Analysis of fluorophore diffusion by continuous distributions of diffusion coefficients: application to photobleaching measurements of multicomponent and anomalous diffusion. *Biophysical Journal* **75**, 557-567 (1998).

14 Huh, D. *et al.* Reconstituting organ-level lung functions on a chip. *Science* **328**, 1662-1668 (2010).

15 Gabriele, S., Benoliel, A.-M., Bongrand, P. & Théodoly, O. Microfluidic Investigation Reveals Distinct Roles for Actin Cytoskeleton and Myosin II Activity in Capillary Leukocyte Trafficking. *Biophysical Journal* **96**, 4308-4318 (2009).

16 Radisic, M. *et al.* High-density seeding of myocyte cells for cardiac tissue engineering. *Biotechnol*

Bioeng **82**, 403-414 (2003).

17 Radisic, M. *et al.* Medium perfusion enables engineering of compact and contractile cardiac tissue. *Am J Physiol Heart Circ Physiol* **286**, H507-516 (2004).

18 Toh, Y.-C. & Voldman, J. Fluid shear stress primes mouse embryonic stem cells for differentiation in a self-renewing environment via heparan sulfate proteoglycans transduction. *The FASEB Journal* **25**, 1208-1217, doi:10.1096/fj.10-168971 (2011).

19 Guo, L. *et al.* The electrophysiological effects of cardiac glycosides in human iPSC-derived cardiomyocytes and in guinea pig isolated hearts. *Cellular Physiology and Biochemistry* **27**, 453-462 (2011).